LABORATORY STUDIES OF WIND ACTION ON WATER STANDING IN A CHANNEL

by

G. M. Hidy

National Center for Atmospheric Research

and

E. J. Plate

Colorado State University

CER65GMH-EJP22

LABORATORY STUDIES OF WIND ACTION ON WATER STANDING IN A CHANNEL

G. M. Hidy
National Center for Atmospheric Research
Boulder, Colorado

and

E. J. Plate
Colorado State University
Fort Collins, Colorado

ABSTRACT

The processes of wave and current development resulting from wind action on initially standing water have been investigated in a wind-water tunnel. The mean air flow over wavy water was examined along with the variation of several properties of the water motion with fetch, water depth, and wind speed. Measurements of phase speed and length of significant waves, the standard deviation of the water surface, the average surface drift, the autocorrelation of surface displacement and the frequency spectra are reported. The experimental results indicate that (a) the air motion in the channel follows a three dimensional pattern characteristic of wind tunnels of rectangul cross-section; (b) wind waves generated in the channel travel downstream at approximately the same speed as gravity waves of small amplitude, provided the effect of the drift current is taken into account; (c) the average drag coefficients for the action of the wind on the water surface increase with increasing wind speed, and these data are reasonably consistent with results of previous investigators; (d) the autocorrelations and frequency spectra indicate that the wind waves in the channel consist of nearly regular primary waves on which are superimposed smaller ripples; (e) energy in the high frequency range in the spectra tends to approach an equilibrium distribution while the lower frequency components continue to grow with increasing fetch; and (f) a similarity shape for the frequency spectra develops. The experiments in this study were not intended to model the processes of interaction between the ocean and the atmosphere. Nevertheless, the small waves generated in the channel appear to be at least qualitatively related to the development of waves on much larger bodies of water.

I. INTRODUCTION

In spite of a long history of effort devoted to the air-water interaction problem, the basic knowledge of the mechanisms for transport processes near the boundary between these two fluids has developed rather slowly. A variety of theoretical and experimental studies have been reported in the literature, but, because of the complexities of the physical processes involved, the detailed nature of the interaction remains inadequately understood.

Most of the experimental studies of air-water interaction have been undertaken on lakes or on the ocean where the conditions of the fluids are highly variable in time and space. These investigations have contributed significantly to the knowledge of the atmosphere and the sea. However, their usefulness in elucidating the fundamental physics of the exchange processes occurring between the two fluids is limited. Therefore, more studies should be carried out under controlled conditions in the laboratory to gain new insights into the mechanisms of transport across the air-water boundary.

Ursell (1956) has reviewed the fundamental laboratory experiments dealing with air-water interaction that were undertaken before 1954. Since the publication of Ursell's paper, a number of new investigations have been reported which included those of Sibul (1955), Cox (1958), Fitzgerald (1963), Schooley (1963) and Hanratty and coworkers (e.g., Cohen and Hanratty (1965)). With the exception of Cohen and Hanratty's work, the experiments performed by these investigators were not designed specifically to verify recent theoretical conclusions, or to serve as a starting point for developing refined ideas about the nature of air-water interaction. With this background in mind, a detailed experimental program has been initiated at NCAR and at CSU to study the relationship between the turbulent flow of air and water in a channel.

Properties of the Fluid Motion

When air moves at moderate velocities over water, a drift current develops, and small waves are generated on the liquid surface. A schematic picture of the development of combined air and water motion along with the growth of waves in a channel is shown in Figure 1. The properties of fluid motion examined in this study are indicated in this drawing. The coordinate system is indicated so that x is the distance downstream, and z is the vertical direction. The mean water surface is given by $z = d$ while the surface displacement from this level is denoted as ξ. The fetch F denotes the distance from the leading edge of the water to a particular point somewhere downstream. In terms of a two dimensional model, the velocity distribution in the water is $u(z)$, and the drift as the water surface is u_o. The air flow is given by $U(z')$, where U_∞ denotes the air velocity at approximately 20 cm above the mean water surface, and $z' = (z - d)$. The wave length $\bar{\lambda}$ and the phase speed $\bar{c}$ denote properties of significant waves.

For the purpose of this study, significant waves will refer to the

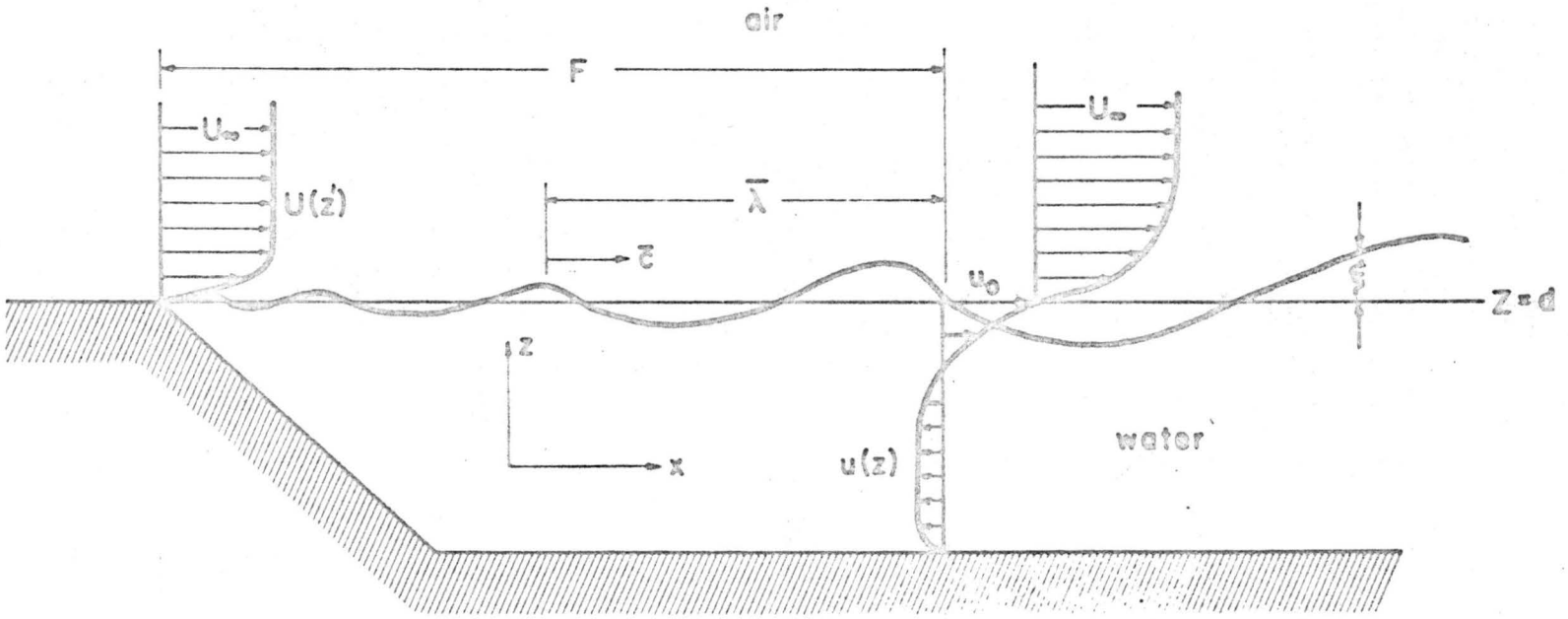

Figure 1. A schematic drawing of air and water motion associated with growing waves on a water surface.

arger regular waves observed at a given fetch. In general, smaller ripples are uperimposed on the larger disturbances.

In this paper, a number of experimental results are discussed which efer to the mean air and water motion as indicated in Figure 1. Measure-nts of the statistical properties of the wind generated waves, including he autocorrelation and spectral density functions, are examined in the light f other properties of the fluid motion. There has been no attempt to model ne ocean-atmosphere interaction with the laboratory equipment. However, it ill be seen that a number of experiments for fluid flow in the channel are t least qualitatively related to the observed small scale interaction between he sea and the atmosphere.

II. EXPERIMENTAL EQUIPMENT AND PROCEDURE

The experiments were conducted in the wind-water tunnel at Colorado tate University. This facility, shown schematically in Figure 2 consists f a tunnel or a closed channel 0.61 m wide by 0.76 m high whose plexiglass est section has a length of about 12 m. During operation, the maximum depth f water is approximately 15 cm. Air is sucked through the tunnel at elocities up to 18 mps by a large axial fan at the outlet. The inlet cone s designed to give a 4/1 contraction ratio. Two fine mesh screens are laced in the inlet cone. Honeycombs are placed just upstream of the outlet iffuser to minimize the axial rotation in the air induced by the fan. loping beaches are placed at the inlet and the outlet to prevent the reflec-ion of waves. The "beaches" are constructed of aluminum honeycomb. The nclines are shaped in such a way that as smooth as possible a transition can e effected in the air-water flow. In this study, the bottom of the tunnel as smooth.

The air flow through the tunnel was measured by a pitot-static tube laced on a carriage in conjunction with a capacitative pressure transducer. he probe could be positioned anywhere in the section of the tunnel from the ottom to a level about 10 cm from the top.

The pressure gradient of the air and the depth of the water were measured very 4 feet down the tunnel with piezometer taps connected to a set of anometers.

Phase speeds and lengths of waves were determined from photographs taken with a movie camera. The length for successive waves was measured from the ovies by comparing the distance between crests with a ruler in the picture. he phase velocities of waves referred to a fixed point were estimated by easuring from adjacent frames the distance traveled by a given crest during he time between successive frames. Time intervals between frames were read ff a timer that was shown in the film.

To measure the change in the height of the water, a capacitance probe as used which is similar to Tucker and Charnock's (1955). This probe con-isted of a 34 gauge magnet wire stretched vertically along the center

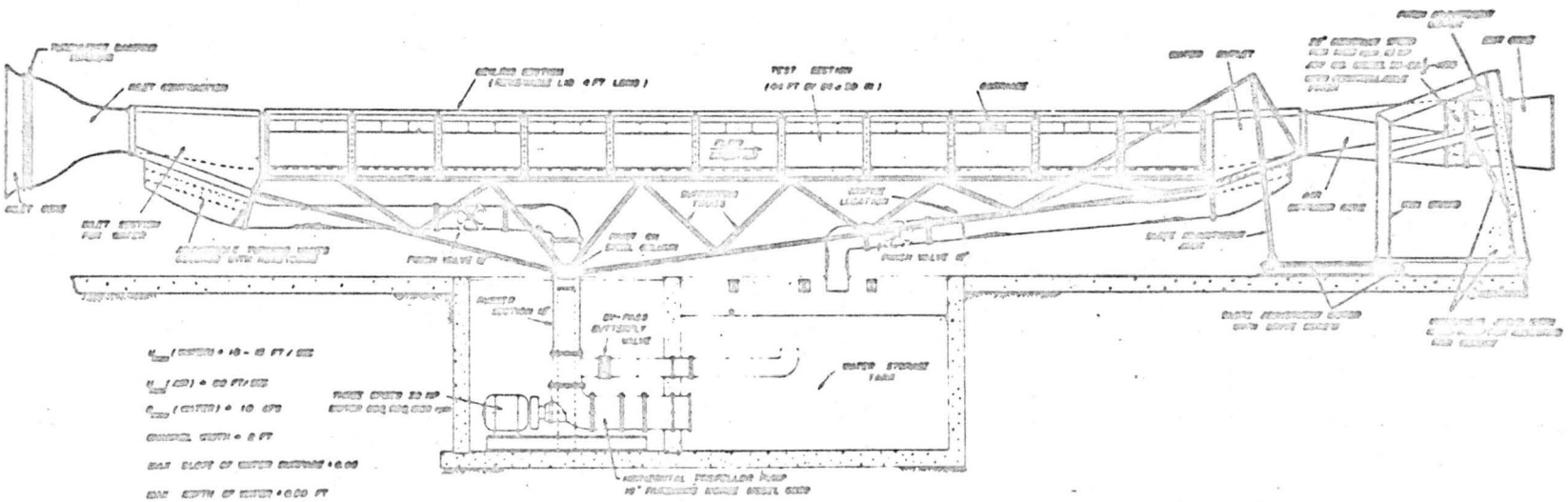

Figure 2. A general view of the wind-water tunnel.

ine of the cross-section of the tunnel. These wires were placed at 1.2 m intervals downstream from the inlet of the tunnel. The wire itself and the water serve as the two plates of a condenser, and the insulation material (Nyclad) on the wire provides the dielectric medium. The capacitance between the wire and the water was measured with an AC excited bridge; the unbalance voltage from the bridge was linearized, amplified and rectified so that a DC output voltage was obtained which was directly proportional to the water depth. The output signal was fed to an oscillograph where the gauge response was continuously recorded during a run. The capacitance bridge-oscillograph combination was calibrated to give a recorded amplitude linearly proportional to the (varying) water depth with a flat response to frequency ($\pm 1\%$) up to approximately 30 cps.

From the continuous records of the surface displacement, data were read off at equal intervals of 0.025 sec. These data were used for obtaining values of standard deviation σ of the surface displacement, the autocorrelations $R(\tau)$ of the surface displacement, and the spectral density function $\Phi(f)$. The computations were carried out on the NCAR-CDC 3600 computer.

It was not possible to obtain the vertical velocity distribution in the water. However, the surface velocity of the water u_o was measured by placing a small slightly buoyant particle on the water and observing the time required for it to move past fixed stations downstream. Values of the surface velocity could then be calculated from the intervals of distance of travel and the time of passage.

In this study, attention was centered on the measurement of the properties of water waves under conditions of steady (mean) air motion. In order to attain steady conditions in the air flow, the wave development, and the set up of water in the tunnel, the fan was started about 15-20 minutes before the photographs, the pitot tube measurements, and the wave amplitude data were taken at a particular location in the tunnel. In cases where wave data were being measured, a sample of a wave train corresponding to the passage of 100-200 waves was taken for a given run.

Samples of wave development were taken for several different conditions. For the condition of water initially standing on a smooth bottom, air velocities taken 20 cm above the water surface, were varied from 0 to 17 mps, and the depth of water was changed from 2.5 to 10 cm. The properties of fluid motion in these cases were observed at distances of approximately 1.8 m to 12 m from the leading edge of the water.

III. THE AIR FLOW OVER THE WATER

Since the air is forced by the fan through the wind tunnel of approximately constant cross section, a pressure gradient develops in the downstream direction. The pressure in the air p_a was found to vary approximately linearly with fetch through the channel. Typical values of the pressure gradient $\frac{1}{\rho w g}\frac{\partial P_a}{\partial x}$ (cm water per cm) as measured in the last 6 m of the

channel are shown in Figure 3. The pressure gradient was found to increase with wind speed, and with depth of the water.

Velocity Distribution in the Air

Measurements of the mean horizontal air motion in the vertical direction and across the channel were taken at several sections for U_{∞} from 6 mps to about 14 mps. Typical data for vertical profiles along the center section of the channel are shown in Figure 4A. The vertical profiles of U(z') indicate that the air flow generally develops a behavior characteristic of turbulent flow in a boundary layer over roughened surfaces. In a few cases, a small kink in the distribution of U(z') was observed which usually appeared at ∿5 cm height above the mean water level. Using pitot tube measurements, Francis (1951) also observed these kinks. Schooley (1963) was able to find the kinks by tracing mean trajectories of bubbles over the waves. However, their measurements indicated that the kinks appeared somewhat closer to the water surface, z' = 2-3 cm. The existence of the kinks in the profiles of air velocity indicate that a jet of high velocity air may sometimes develop over wavy water in channel flows. To the authors' knowledge, however, with the possible exception of Sheppard (1952), this phenomenon has not been observed with any measurements over water in the atmosphere.

Typical measurements of the horizontal distribution of velocity are shown in Figure 4B. These data are representative of flow in wind tunnels of rectangular cross-section. It is interesting to note that the boundary layers associated with the side walls can become rather thick. This thickening had no apparent effect, however, on the development of significant waves in the channel. The waves still exhibited a nearly linear crest moving approximately normal to the mean wind direction.

The lines of constant air velocity plotted for a given cross-section reveal an interesting feature of the channel flow as shown in Figure 5. Because of a secondary circulation in the tunnel, the lines of constant velocity are squeezed down in the corners of the cross-section. This has been observed previously for flow in rectangular ducts (e.g., Schlichting (1960)). However, the effect appears to become somewhat more pronounced when fluid flows over a moving boundary in the CSU channel.

The three dimensional structure of the air flow does not visibly affect the waves generated on the water surface. However, the pressing of the air moving at higher speeds down along the walls seems to be transmitted to the horizontal velocity in the water. Measurements of the horizontal distribution of velocity in moving water show two maxima developing just underneath the "ears" of the constant velocity curves drawn in Figure 5. Hence, strictly speaking, the velocity in the air and in water should be written as U(y,z'), and u(y,z), instead of U(z'), and u(z). However, for the purposes of this discussion the motion of the air and the water will be treated as two dimensional.

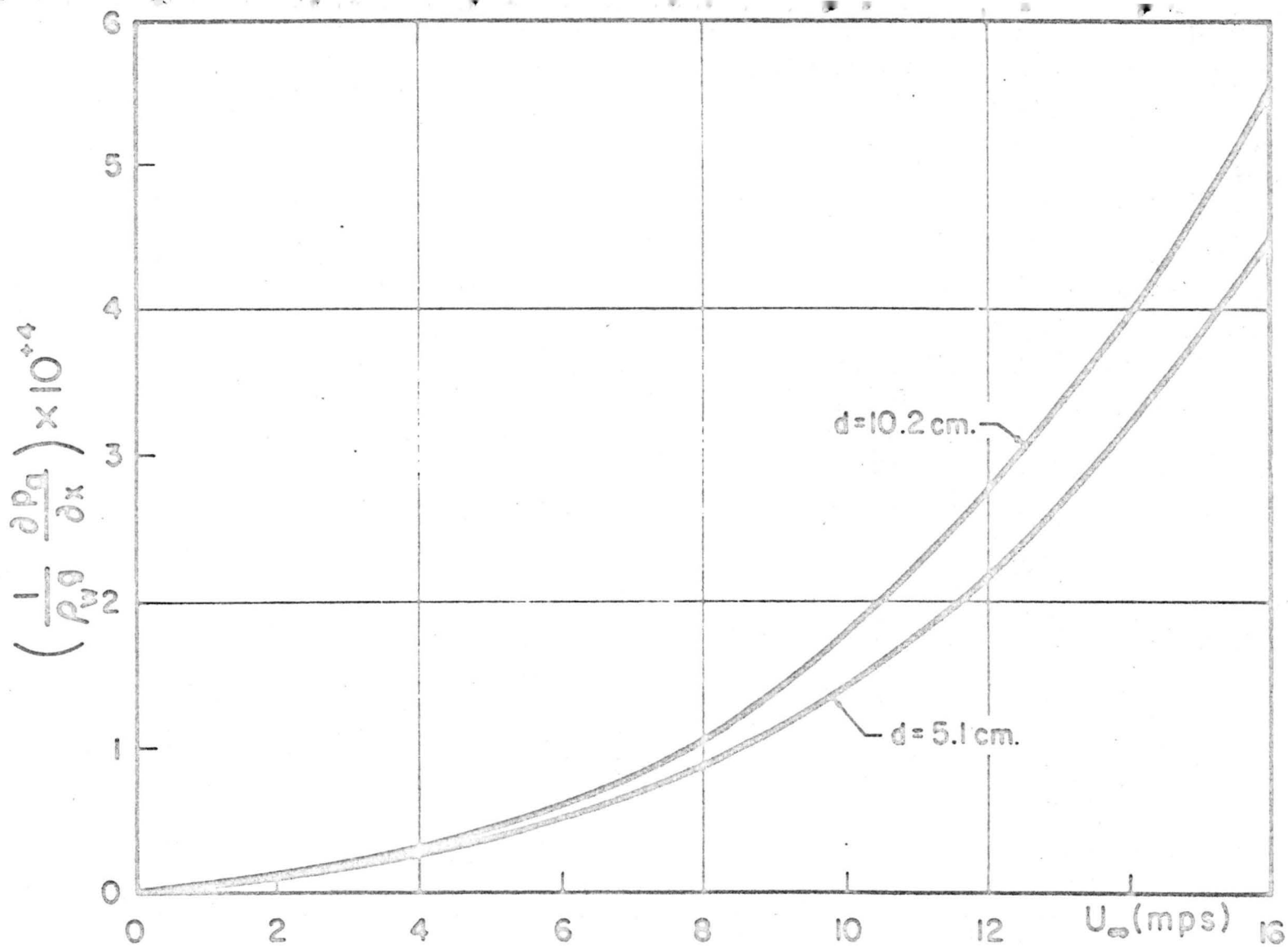

Figure 3. Variation in the pressure gradient in air with air speed in the wind-water tunnel. The pressure gradient is given in terms of length of water per length of channel.

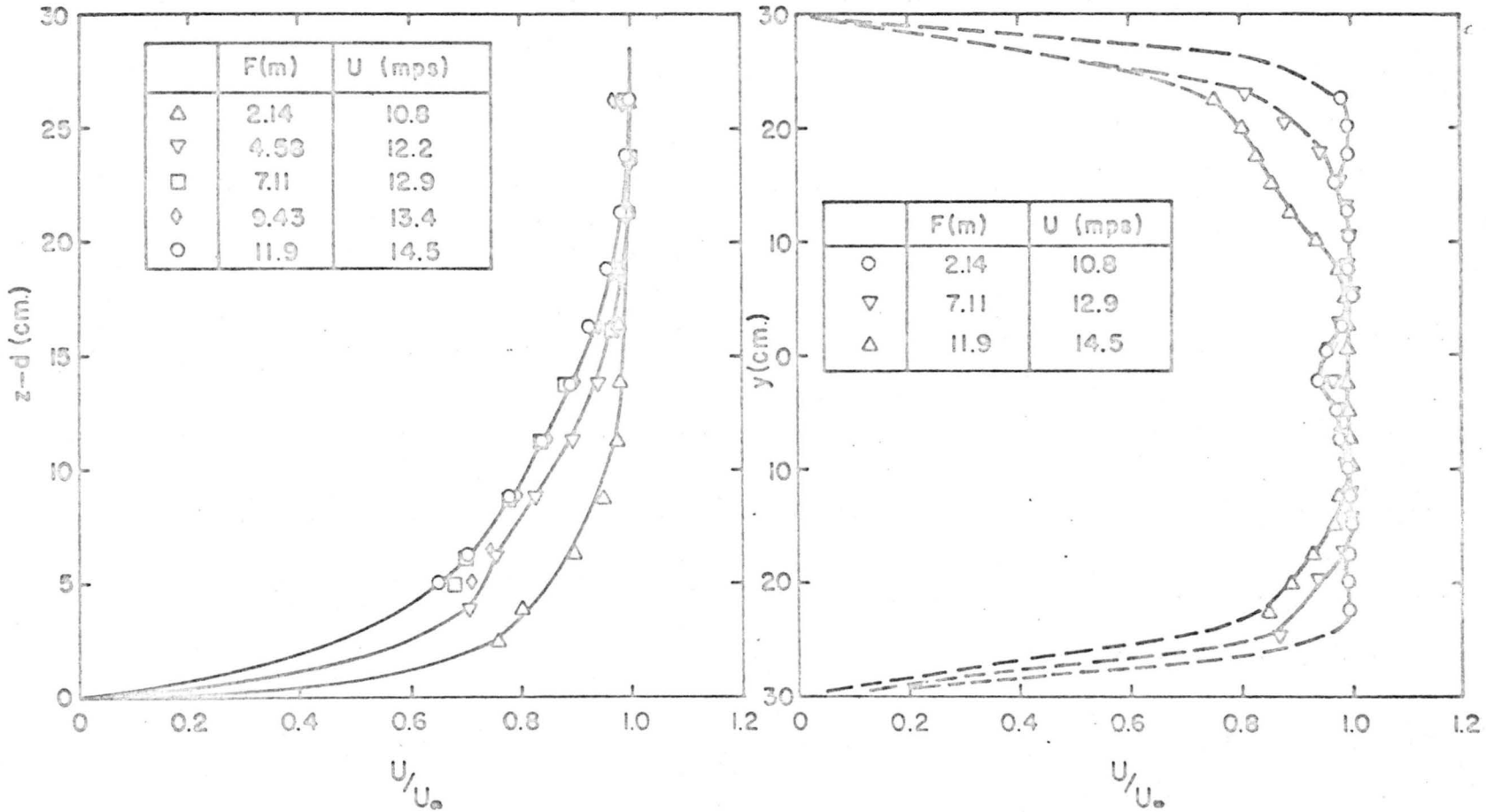

Figure 4. Typical distributions of air flow in the wind-water tunnel.
A. Vertical profiles taken along the center section, and
B. Horizontal profiles taken at (z-d) ≈ 20 cm.

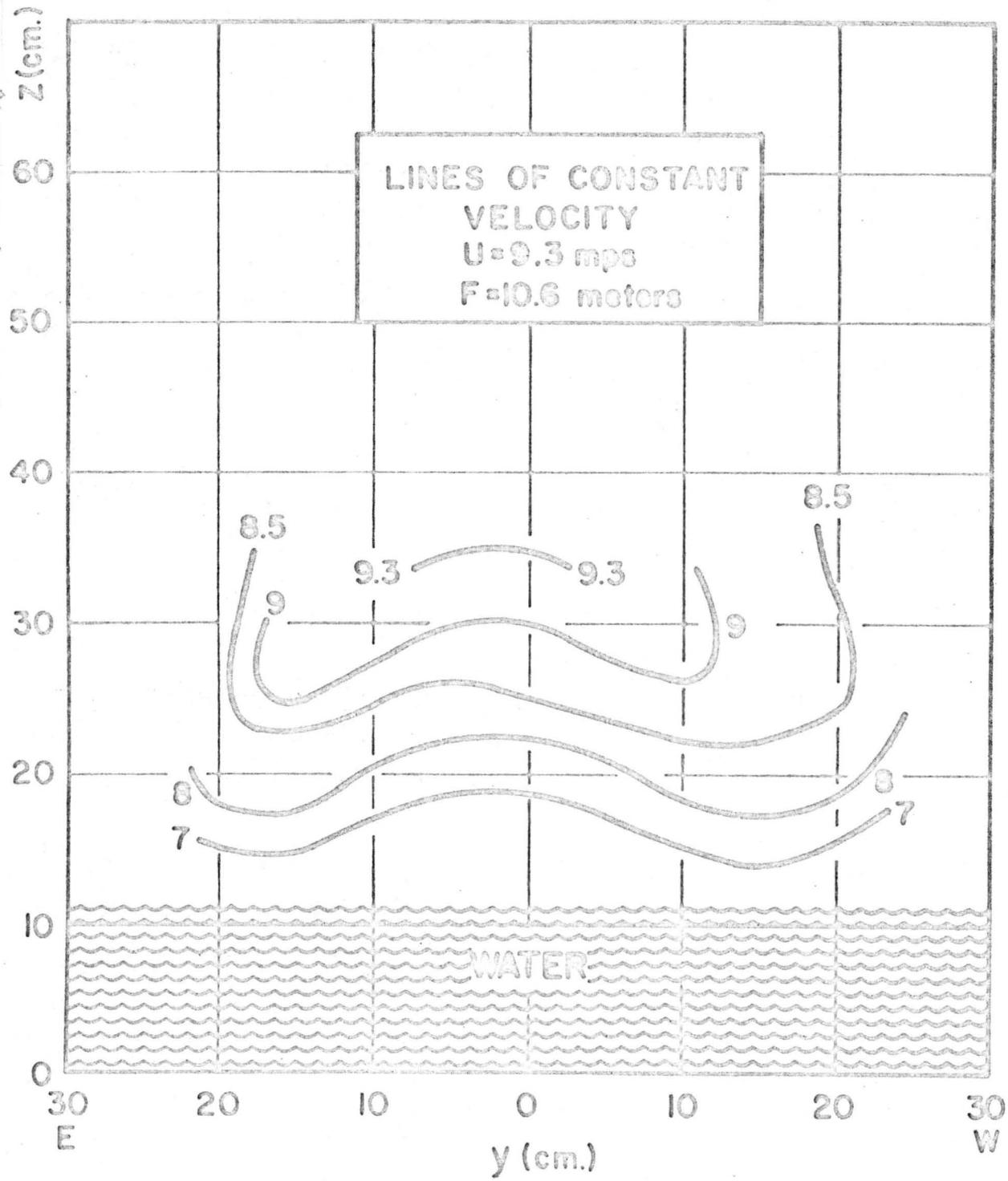

Figure 5. Distribution of air velocity at a given cross-section in the channel.

The vertical profiles for air velocity taken for increasing F along the center line of the tunnel were found to fit the form:

$$\frac{U}{U_\infty} = \left(\frac{z - d}{\delta} \right)^{1/n}$$

where δ is the thickness of the boundary layer as defined by the value z' where $U(z') = 0.99U_\infty$. Over a wide range of fetch, and for $6.1 < U_\infty < 13$ mps the data taken in the channel fit Eq. (1) where $n = 4.5$. This similar distribution is shown in Figure 6. Several typical values of δ are given in Table I. The shape corresponding to Eq. (1) with $n = 4.5$ is frequently found in wind tunnel data for flow over moderately rough surfaces.

Air Flow Close to the Waves

One of the purposes of this study is to examine the nature of the air flow close to the water boundary. A key problem in this work centers around the question of separation of flow to the leeward of the wave crests (Ursell (1956)). Furthermore, recent theories for energy transfer to the waves from the air place strong emphasis on the behavior of the region where air velocity equals the phase speed of waves. For waves generated in the tunnel this zone is very close to the water surface, much closer than can be reached with a fixed probe. That is, the present equipment can only measure average velocities in the air within about 1 cm of the crests of the highest waves. To observe the nature of the air motion near $U = \overline{c}$, and to trace the presence of separation, the probe must be placed much closer to the oscillating water surface than the fixed probe will permit. Therefore, a moving probe has been designed which will follow the significant waves and maintain approximately a constant level above the water surface. The schematic picture of the design, worked out by one of the authors, is shown in Figure 7. The probe is maintained at a constant level above the water by a servo-driven mechanism activated by the depth gauges. This system is currently under construction, and we expect to begin obtaining data from it sometime next year.

IV. PROPERTIES OF THE WAVES

Over a wide range of air flow which follows the patterns described in sec. III, only small gravity waves and capillary ripples were generated on the water standing in the channel. Although the air reached speeds greater than 12 mps, breaking of waves, in the sense of forming white caps, was not observed. At high air velocities droplets of spray were observed being shed from crests of the larger waves, but the waves did not become sharp crested as seen in "fully developed" seas.

Up to wind speeds of about 3 mps, taken about 20 cm above the water, no waves appeared on the water surface. However, very small oscillations of the entire water surface could be observed in this range of air flow by watching variations in reflected light on the water. Above 3 mps, ripples began to form near the leading edge of the water. These small disturbances

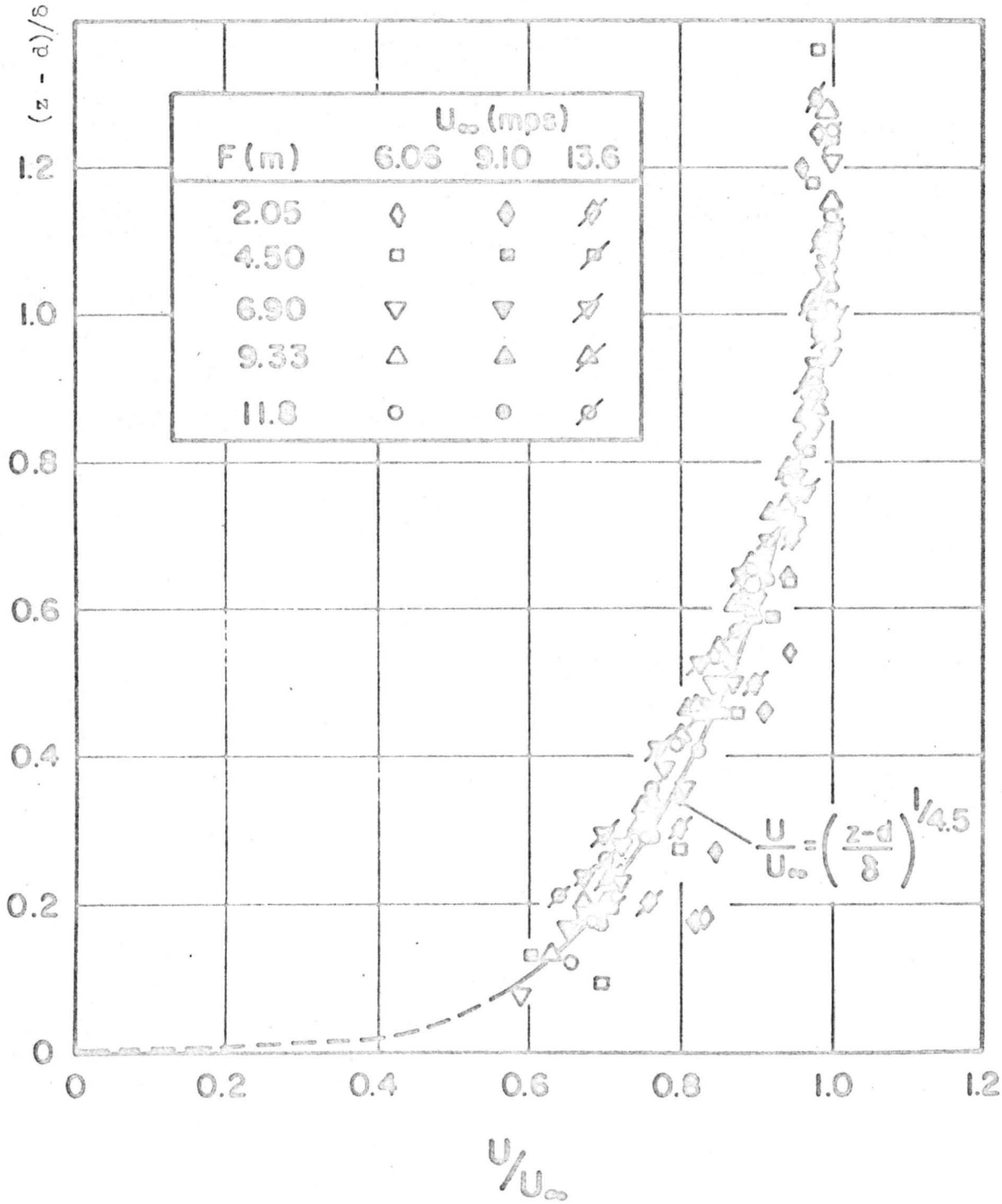

Figure 6. A similarity distribution for the air velocities along the center section of the tunnel.

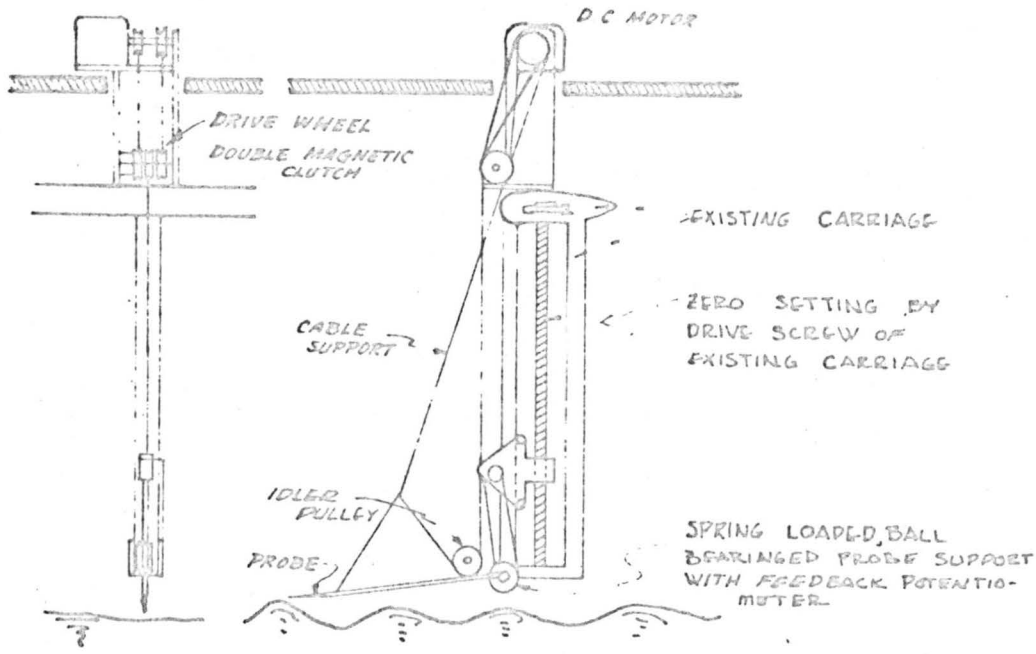

SCHEMATIC DESIGN OF MECHANICAL SYSTEM

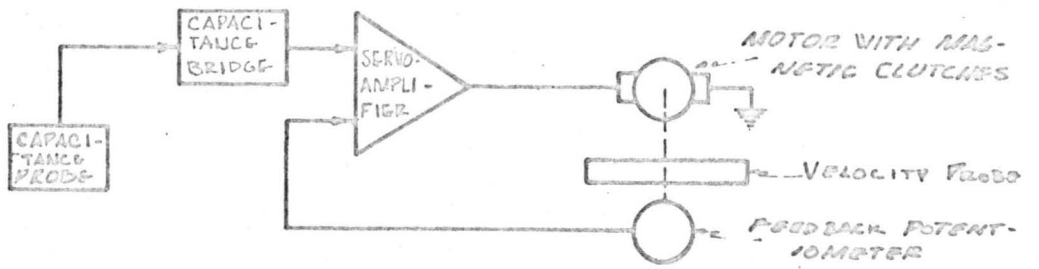

SCHEMATIC DESIGN OF ELECTRICAL SYSTEM

Figure 7. The design of the system for positioning instrument probes near the water surface.

ad wave lengths of 1 - 3 cm. Their direction of propagation was primarily rmal to the wind direction. As the wind speed increased, the ripples itially present became larger in amplitude and height. Under the action the steady air motion, the waves traveled downstream at an increasing peed, growing in amplitude and length. For wind speeds in the range U_{oo} = 3-6 mps, significant waves were observed to run with crests approximately rmal to the wind direction, with smooth windward surfaces, and rippled leeard surfaces. Above 6 mps, capillary ripples were noted on both the windard and the leeward sides of the significant waves. At any given point wnstream from the inlet, groups of 5-20 small gravity waves of nearly the me period passed by. These groups were separated by relatively calm regions small ripples having varied periods. The existence of groups of waves eparated by relatively calm water is probably related to interference between fferent components of the wave train, giving an appearance of "beats."

The growth with fetch of waves in the channel is reflected in two characeristic lengths, the standard deviation σ and the wave length $\bar{\lambda}$ e increase with F and U_{oo} of σ and $\bar{\lambda}$ is shown in Figure 8. The effect depth is also shown in the drawing. Decrease in depth tends to reduce the ve length, and the standard deviation of the (larger) waves generated at gher wind speeds. Our data for σ and $\bar{\lambda}$ were compared to those reported Sibul (1955). For a given value of U_{oo} and d, the results of both these udies appeared to be essentially the same.

Two characteristic velocities are associated with the water motion. These e the surface velocity u_o, and the phase speed of significant waves c_e. The ange with F, U_{oo} and d of these properties is shown in Figure 9. For a ven wind speed, the surface drift remains nearly constant over the range of shown, except near the ends of the channel. The wave speed c_e is approxitely independent of depth down to 5.1 cm, but it increases with both U_{oo} d F.

Keulegan (1951) found that the ratio of the drift velocity u_o to the ad speed could be correlated with the Reynolds number $Re_d = u_o d/\nu_w$, ere ν_w is the viscosity of the water. In his calculations, Keulegan ed an air speed averaged over the cross section of his channel, U_{avg}. Goodwin 65) found that $U_{avg} = 0.85\ U_{oo}$ for the data in the CSU channel. Using this lation, the values of u_o have been plotted with Re_d as shown in Figure 10. drift velocities found in this study are correlated satisfactorily in terms Re_d. Our data fall about 30 percent lower than Keulegan's curve for wavy ver. The difference between these two studies may be accounted for in three ys. First, if it is assumed that the mass flow of water and air are related each other and not the velocities, the momentum ratio, $\rho_w u_o/\rho_a U_{avg}$ ould be used in this correlation. Keulegan's data were taken at sea level ile the CSU measurements were made at nearly 1800 m altitude. If our data corrected for the decrease in air density with altitude, they will fall ut 12 percent below Keulegan's curve. The remainder of the difference tween these experiments may be related to (a) the effect of non-uniformities u_o in the y-direction resulting from the nature of the air flow shown in gure 5, and (b) the fact that Keulegan used a value of u_o averaged over the gth of his channel while our values of u_o are taken locally. The effect (b) should be small, however, since u_o varies little with fetch.

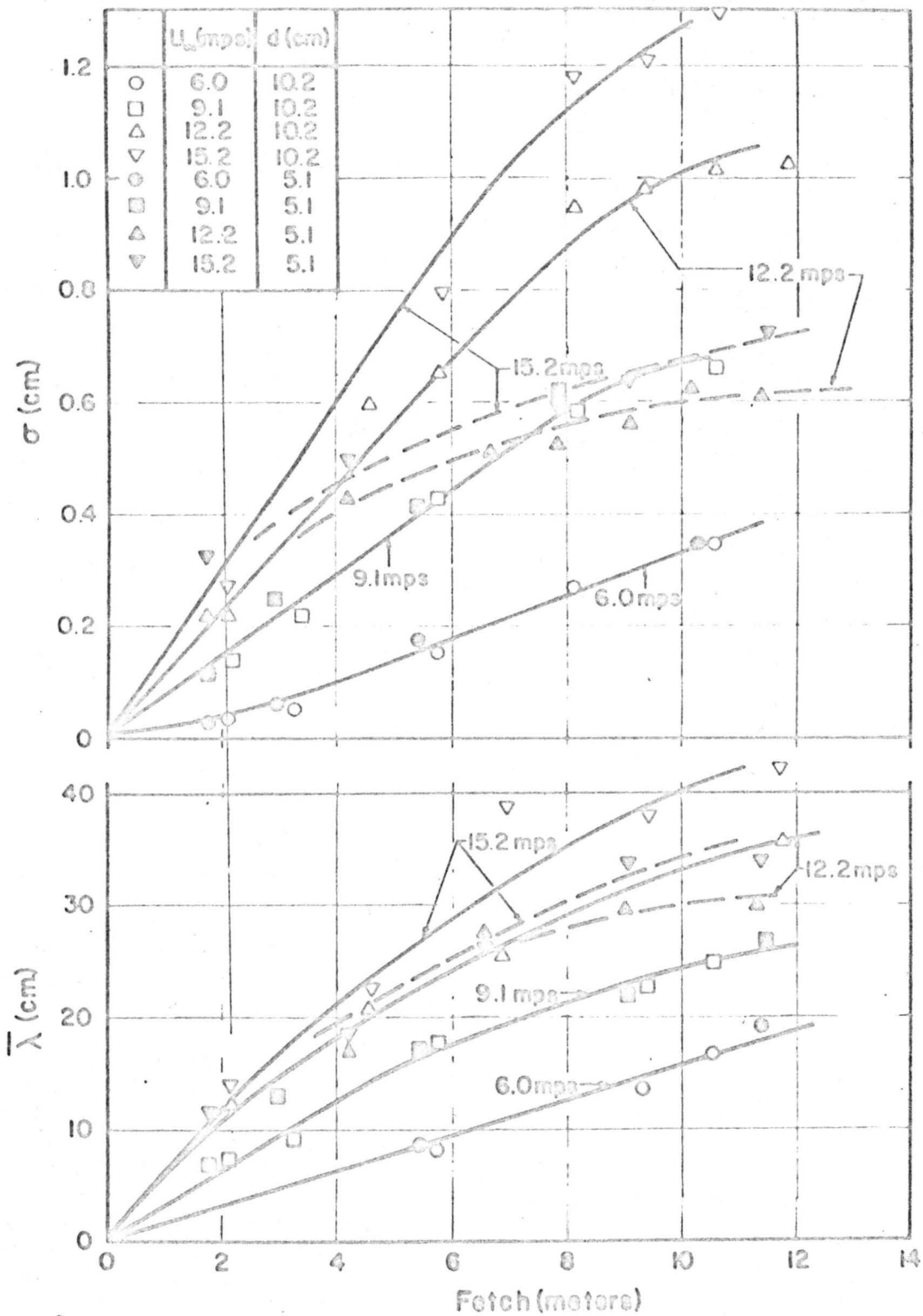

Figure 8. Variation in characteristic lengths of surface waves with fetch and water depth.

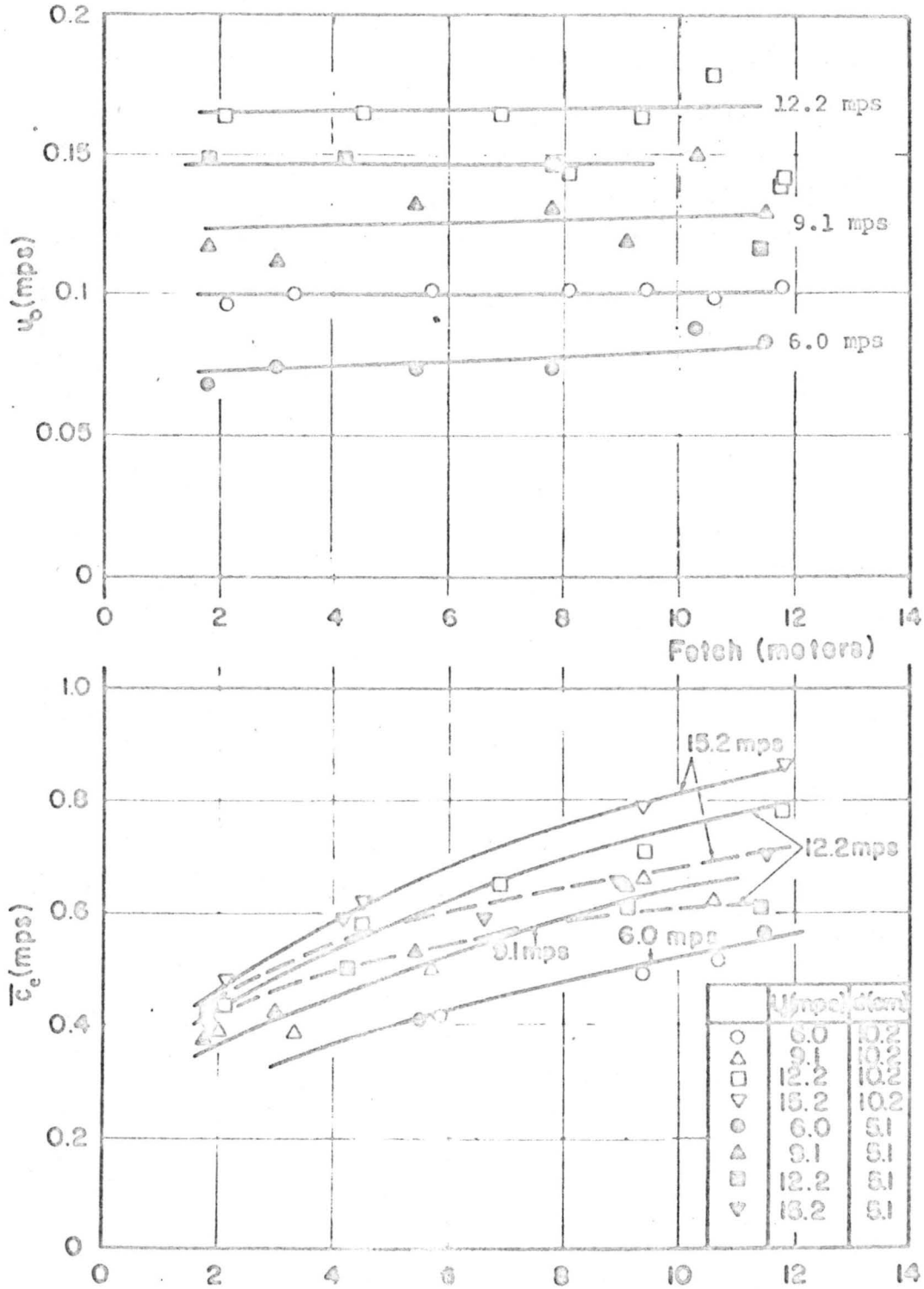

Figure 9. Variation in characteristic water velocities with fetch and depth.

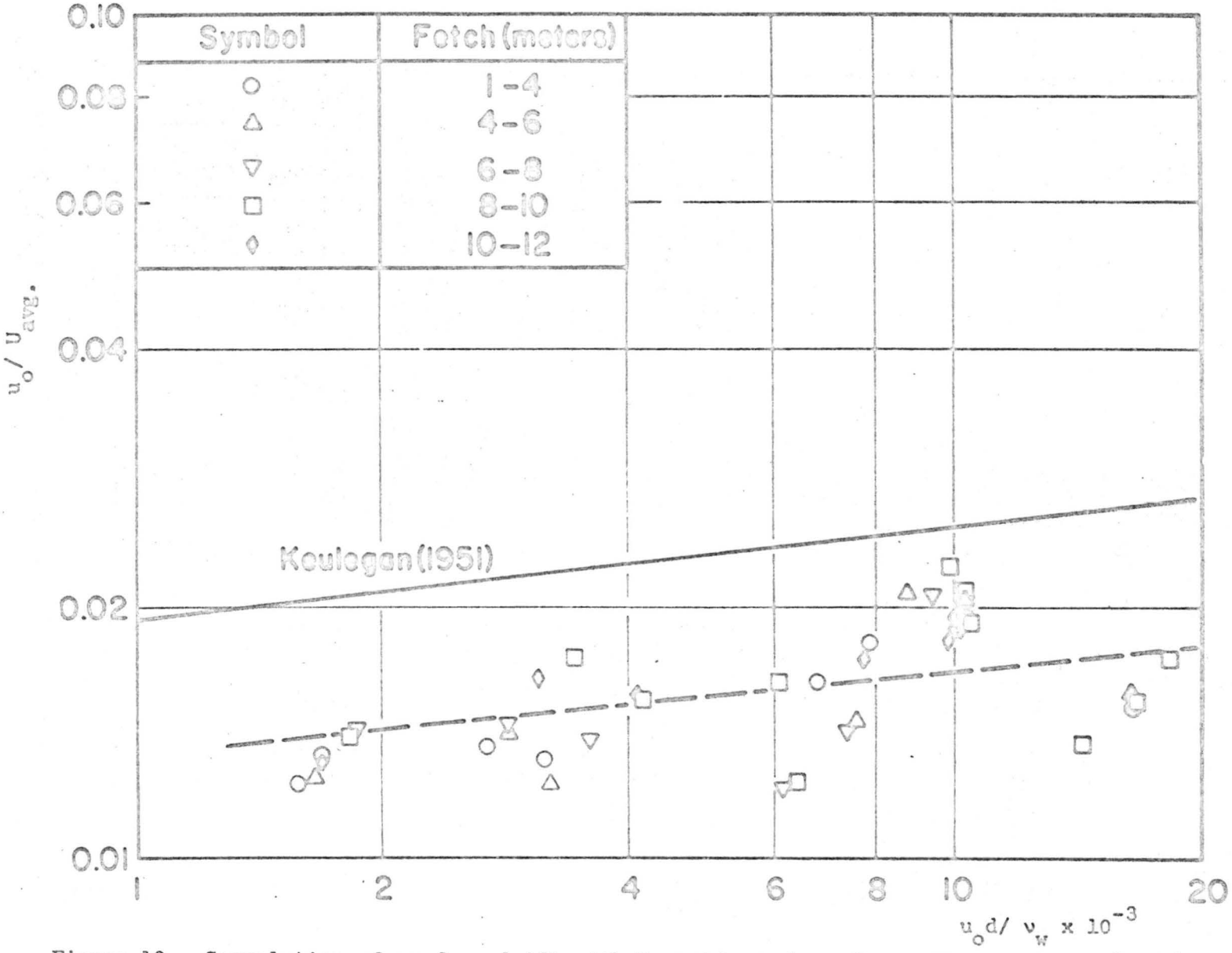

Figure 10. Correlation of surface drift with Reynolds number, Re_d, after Keulegan (1951).

The Phase Speed and the Drift Current

The phase speed of significant waves $\bar{c}_e$ as measured with respect to a fixed point was compared with values calculated from the theory for small amplitude gravity waves. The theoretical phase speed is:

$$c_o = \left[g\bar{k}^{-1} \tanh(\bar{k}d) \right]^{\frac{1}{2}} \qquad (2)$$

where $\bar{k} = 2\pi/\bar{\lambda}$. In all cases, the values of $\bar{c}_e$ were larger than values calculated by Eq. (2). This effect has also been observed by Francis (1951) and Cox (1958). Francis qualitatively accounted for the deviation by considering an increase in wave velocity associated with the surface drift, and the fact that the waves are finite in amplitude. Cox, on the other hand, attributed the difference to the combined effects of finite amplitude, orbital velocity of low-frequency wavelets, drift currents, and dynamic effects of the wind. Cox only analyzed in detail the finite amplitude effect as calculated by Sekerzh-Zenkovich (1956). Cox found that the finite amplitude effect could only explain his observed increase in phase velocity for waves larger than $\bar{\lambda} \approx 7$ cm. The observed differences in phase speed for wavelets of length smaller than ~ 7 cm could not be accounted for by the influence of finite amplitudes alone.

For strict comparison to $\bar{c}_e$, c_o should be corrected for the mean motion of the water and not the surface drift since c_o should be measured relative to an average transport in the water. Because the orbital movement of water particles associated with the waves extends downward to some depth, the surface drift u_o is not the proper correction factor. The correction should be proportional to a weighted average water velocity over some depth below the surface.

Lilly (1964) has proposed a drift correction for waves traveling on water at finite depth. Assuming that the vertical profile of the drift current is parabolic (laminar flow), and that the waves have infinitesimal amplitudes, Lilly found that

$$\bar{c}_T = c_o \left\{ 1 + \frac{u_o}{c_o} \left[1 + \frac{3}{2(\bar{k}d)^2} - \left(\frac{1 + 2\cosh(2\bar{k}d)}{(\bar{k}d)\sinh(2\bar{k}d)} \right) \right] \right\} \qquad (3)$$

For deep water, $\bar{k}d \to \infty$ and Equation (2) implies that the waves travel with the surface flow only (i.e., $c_T = c_o + u_o$). However, for shallow water, $\bar{k}d \to 0$, and Eq. (3) predicts, as expected, that $\bar{c}_T \to c_o$.

The values of $\bar{c}_T$ as calculated by Eq. (3) were compared to the corresponding experimental data, and the results are shown in Figure 11. Experiment and theory agree within $\pm$ 15 percent. This error is approximately that expected on the basis of experimental errors in estimation of $\bar{c}_e$, and $\bar{c}_T$ using $\bar{\lambda}$ and u_o.

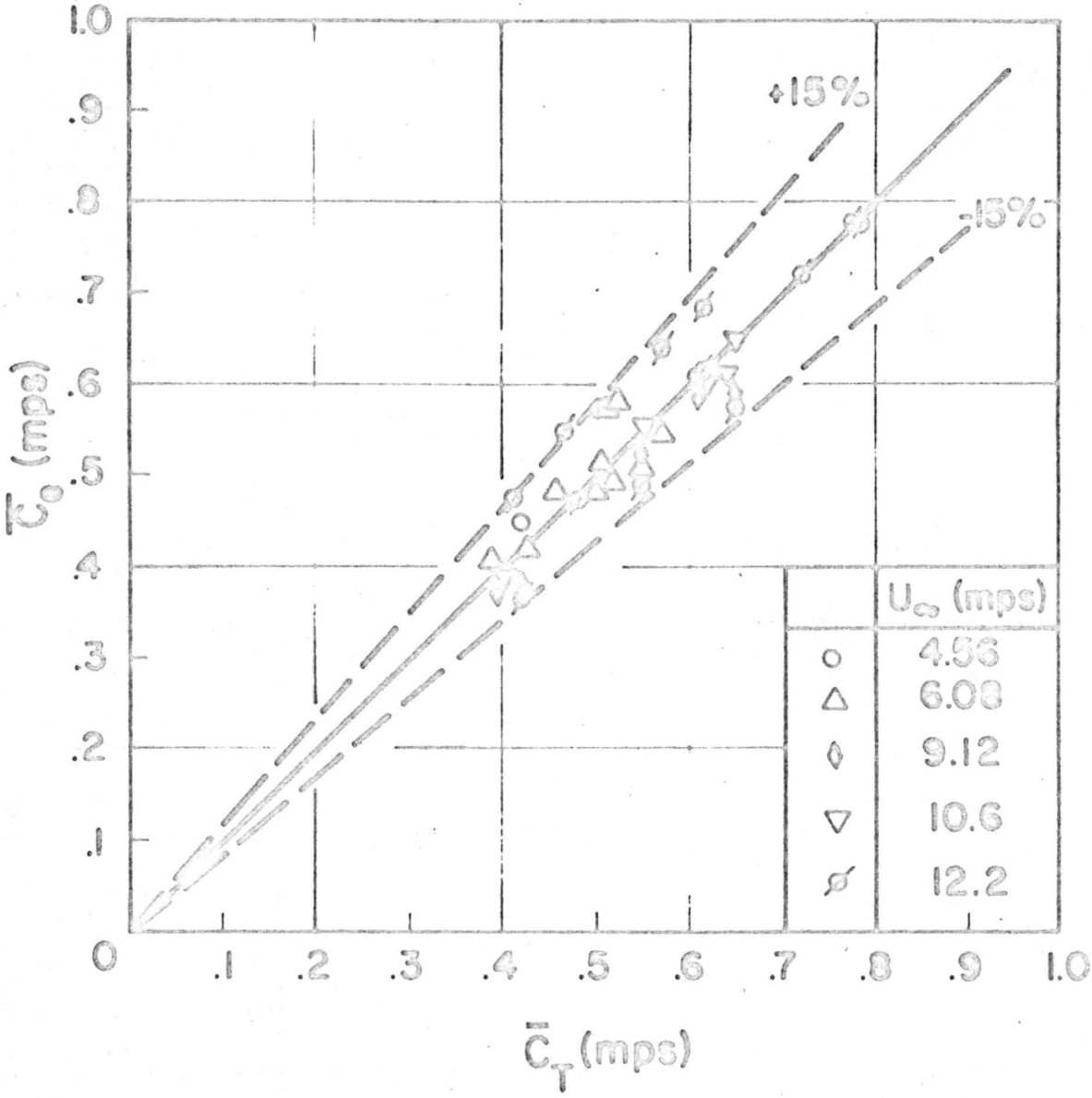

Figure 11. Comparison between experimental values of the phase speed of significant waves and values calculated by Lilly's theory.

Systematic deviations between $\bar{c}_e$ and $\bar{c}_T$ might be expected since both the effect of surface tension and of finite wave amplitude were not considered in deriving Eq. (3). The correction in $\bar{c}_T$ for surface tension in deep water waves was found to be negligible for the experimental observations. However, the Stokes correction of c_T for gravity waves of finite amplitude (e.g., Lamb (1932)) could vary from 1 percent to 11 percent (increase) if it is assumed that the amplitude of significant waves is $3.0\,\sigma$ (e.g., Sibul 1955)). Thus, Lilly's equation would give values of $\bar{c}_T$ somewhat larger on the average than the experimental data.

The effect of finite amplitudes in the wind waves may be offset partially by the influence of turbulence in the water. Dye traces of the motion in the water indicate that the water flow was turbulent and not laminar. The use of a turbulent velocity profile having a steeper gradient near the surface than the parabolic curve but having the same drift velocity at the surface would result in a smaller correction factor for drift than predicted by Eq. (3).

These results indicate that the significant wind waves on the water in the channel travel relative to a mean drift approximately as gravity waves of small amplitude. The waves tend to propagate in this way in spite of the steady pushing of the moving air.

Shearing Stress on the Water

An important parameter for measuring the action of the wind on the water is the shearing stress on the water surface, τ_s. This is often calculated in terms of the drag coefficient

$$C_s = \tau_s / \rho_a U^2 \quad , \tag{4}$$

where ρ_a is the density of the air. An average value of the shearing stress at the surface $\bar{\tau}_s$ can be estimated for the data of the present study by taking a force balance on the body of air, or the body of water in the channel at a given time. The shearing stress on the (smooth) walls, on the top of the tunnel and on the bottom can be estimated in well known ways (e.g., Schlicting (1960)). Then the stress $\bar{\tau}_s$ can be calculated from differences between the pressure gradient (on the set up of water), and the shear forces on the walls, bottom and the top. This has been done for our data by Goodwin (1965). His results are expressed as the average drag coefficient based on the average air velocity in the tunnel as defined by:

$$\bar{C}_s = \bar{\tau}_s / \rho_a U_{avg}^2 \tag{5}$$

Estimates of $\bar{C}_s$ as they vary with U_{avg} are shown for two different depths in Figure 12. For comparison, the data of other investigators, Francis (1951), Keulegan (1951), and Fitzgerald (1962) are also indicated. Goodwin's calculations by the force balance technique as applied to the water and the

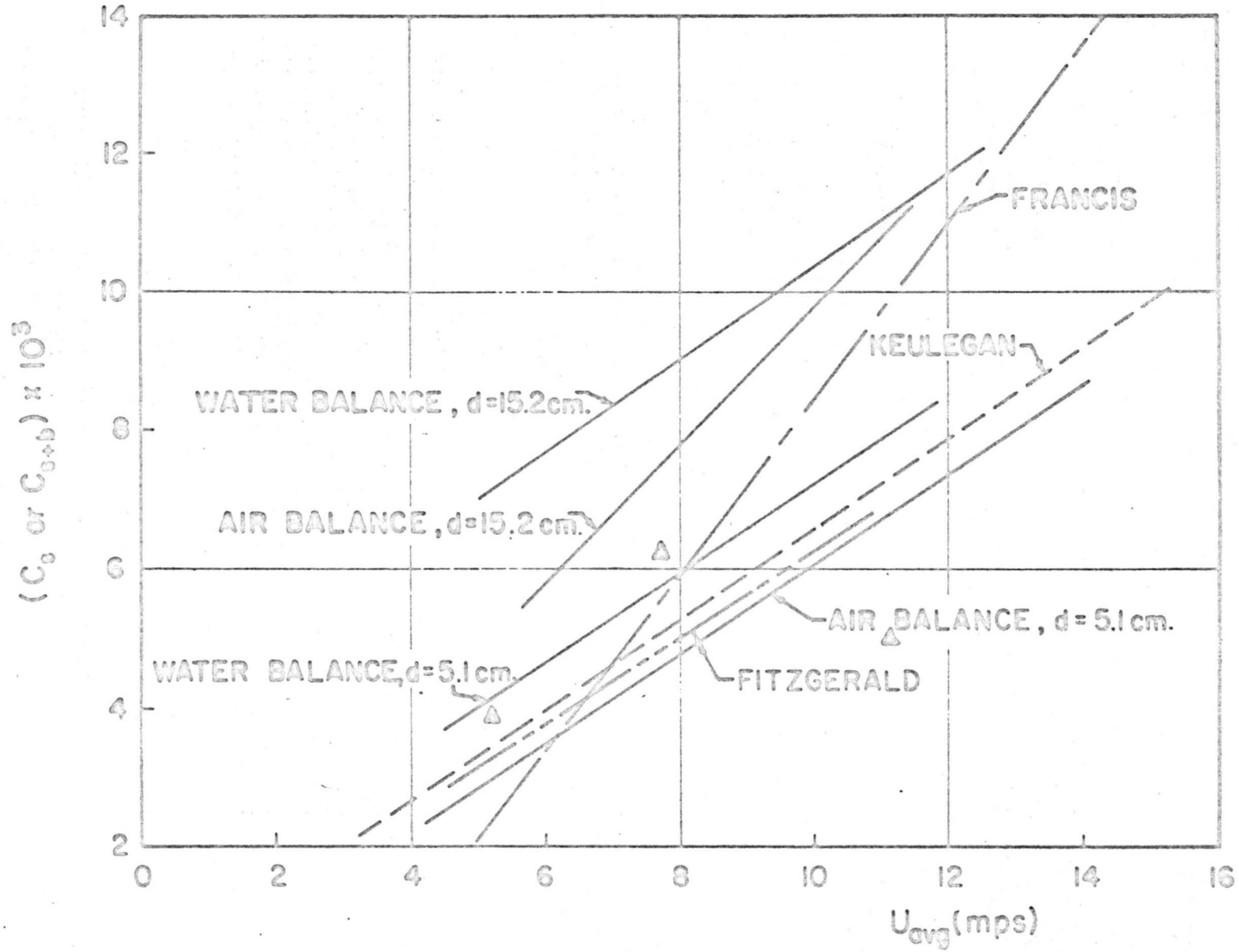

Figure 12. Mean drag coefficients on the water surface. The triangular points refer to averaged local coefficients as calculated from Eq. (7).

air are not the same, but some differences are expected, which will result from estimations of the stresses on the walls of the tunnel. The data for d = 5.1 cm appear to be in reasonably good agreement with the results of Keulegan and Fitzgerald. However, Francis' results show a steeper increase in $\overline{C}_s$ with U_{avg}.

It is worth noting here that all of the values of $\overline{C}_s$ correspond to the case where the channel bottom is smooth. Fracis' calculation includes the effect of the average bottom shear $\overline{\tau}_b$ as well as the surface shear in his value of the drag coefficient (i.e. $\overline{C}_{s+b} = (\overline{\tau}_s + \overline{\tau}_b)/\rho_a U_{avg}^2$). This is equivalent to assuming that the ratio $\overline{\tau}_b/\overline{\tau}_s$ is zero for turbulent flow in the water. Fitzgerald based his data on the same assumption. However, Keulegan took $\overline{\tau}_b/\overline{\tau}_s = 0.25$ in estimating $\overline{C}_s$ only. In view of this, it is not clear why Fitzgerald's data for $\overline{C}_{s+b}$ show close agreement with the results of Keulegan and Goodwin for $\overline{C}_s$ while Francis' results display a considerably larger variation of $\overline{C}_{s+b}$ with U_{avg}. It is also difficult to understand why Goodwin found such a large change in $\overline{C}_s$ with depth of the water. At present, this conclusion cannot be checked with the findings of other investigators because their results apply to one water depth only.

Local values of the drag coefficient ($C_s' = \tau_s/\rho_a U_\infty^2$) can also be estimated from our data. Although evaluation using the assumption of the logarithmic profile cannot be applied, the momentum integral technique can be used (e.g., Schlichting (1960)). The relation for C_s' by this method is:

$$C_s' = \frac{1}{U_\infty^2}\left[\frac{d(U_\infty^2\theta)}{dx} - \frac{\delta^*}{\rho_a}\left(\frac{dp_A}{dx}\right)\right] \qquad (6)$$

where δ^* is the displacement thickness:

$$\delta^* = \frac{1}{U_\infty}\int_d^{z''}(U_\infty - U)\,dz' \quad , \qquad (7)$$

θ is the momentum thickness:

$$\theta = \frac{1}{U_\infty^2}\int_d^{z''}U(U_\infty - U)dz' \quad , \qquad (8)$$

and z" is the value of (z-d) where $U = U_{\infty}$.

To accurately obtain values of C_s' from Eq. (6), the slope of U_{∞} and values of δ^* must be well established. The contribution of $(U_{\infty}-U)$ to the integrals in Eqs. (7) and (8) depends strongly on the region of the

vertical profile where the curvature is greatest. In our measurements, this is poorly defined because the curving portion of U(z') lies too close to the water for accurate measurement with the fixed probe. Thus, the use of Eq. (6) with Eqs. (7) and (8) can be expected to give only an order of magnitude estimate of C_s'.

In addition to the problem of using the experimental data in Eqs. (7-9), the application of a definition for proper air velocity must be considered. Eqs. (7-9) apply to flow over a solid boundary. When the boundary is moving and waves are superimposed on this motion, the air speed relative to fixed coordinates may be an incorrect estimate for U(z'). Two other systems of velocity coordinates can be used. The air velocity relative to the surface drift may be a better system, or as Benjamin (1959) has noted, the motion relative to the phase speed c may be better than the fixed system of reference. Introduction of either one of these reference velocities will affect the definitions of δ^* , θ , δ , and C_s'.

In spite of these difficulties, it is useful as a first approximation to apply Eqs. (7-9) for evaluating C_s'. Calculations of the local drag coefficients based on the data for U(z') were made, and some typical results for δ^* , θ , and C_s' are shown in Table I. These results indicate that C_s' decreases somewhat with fetch, but tends to increase with wind speed. The decrease with fetch is typical of the variation in C_s' in the context of a growing boundary layer over a solid surface.

TABLE I

F(meters)	Nominal Average Air Speed (mps)	U_{∞} (mps)	δ (cm)	δ^* (cm)	θ (cm)	$C_s' \times 10^3$
2.14	5.2	4.76	7.12	2.00	0.682	3.39
4.58		5.20	14.0	2.80	1.23	2.65
7.03		5.48	17.8	4.04	2.08	2.33
2.14	7.7	7.20	13.7	2.97	1.44	5.66
4.58		7.95	19.6	4.60	2.28	4.32
7.03		8.80	22.8	5.43	2.82	3.31
2.14	11.6	10.8	12.7	3.18	1.40	5.31
4.58		12.1	19.3	4.90	2.35	3.75
7.03		12.8	21.6	5.68	2.74	2.50

Using the nominal average velocity (0.85 U_{∞} measured at large fetch), estimates of $\overline{C}_s$ were calculated by averaging each set of three values of C_s' for the ranges of U_{∞} in Table I. As a comparison to Goodwin's results, the three estimates of $\overline{C}_s$ by this method are plotted as triangular points in Figure 12. The data for $\overline{C}_s$ by two different calculations check reasonably well for the 5.1 cm depth of water.

The velocity profiles for air were taken primarily at 15.2 cm water depth, but there should be little change in air flow at 5.1 cm. One should bear in mind, however, that $\overline{C}_s$ calculated from the data in Table I represents $\overline{\tau}_s$ in a narrow slice along the center section of the channel. Strictly speaking, Goodwin's estimates of $\overline{\tau}_s$ include the variation of C_s' in the y direction. From Figure 5, it is clear that the shear on the water surface near the maxima in the cross-sectional distribution of air velocity will be larger than that at the center section. This may account for the differences between values of $\overline{C}_s$ at d = 15.2 cm as estimated by Goodwin's method and the momentum integral technique.

V. WAVE SPECTRA

Autocorrelation Functions and the Frequency Spectra

The time correlations between displacements of the water surface were calculated from the digitized depth gauge data. The autocorrelation function $R(\tau)$ is defined as:

$$R(\tau) = \overline{\xi(t_1)\ \xi(t_2)}\ , \qquad \tau = t_2 - t_1 \tag{10}$$

where $\xi(t_1)$ and $\xi(t_2)$ are surface displacements taken at the same point for two different times, t_1 and t_2. The averaging technique in Eq. (10) was carried out after the method given in Blackman and Tukey (1958).

The function $R(\tau)$ for waves in the channel was found to exhibit certain interesting features. A typical example is shown in Figure 13. $R(\tau)$ was generally found to oscillate regularly about the $R(\tau) = 0$ line with increasing τ. Its amplitude decreased sharply initially, but it became fairly steady at higher values of τ, though sometimes it varied slowly as if a lower harmonic was present. The behavior of $R(\tau)$ suggests that there is a tendency for the mutual action of the two fluids to force a nearly periodic, regular disturbance to develop on the water at a given fetch in the channel. On the regular waves are superimposed small, random disturbances which are related to the larger values of $R(\tau)$ for small τ. This, of course, is precisely the physical picture which developed from visual observations of the development of the significant waves.

It is well known that the autocorrelation of a periodic function of period P is another periodic function with period P and a zero mean. Hence, the period of the significant waves can be estimated from the zero crossings of the autocorrelation function at large values of τ where the effects of the random component are small. As seen in Figure 13, the components of "noise" tend to damp out rapidly, so that the period of the significant waves also can be calculated approximately from zero crossings of $R(\tau)$ over the whole range of τ. Typical values of 1/P found in this manner are listed in Table II.

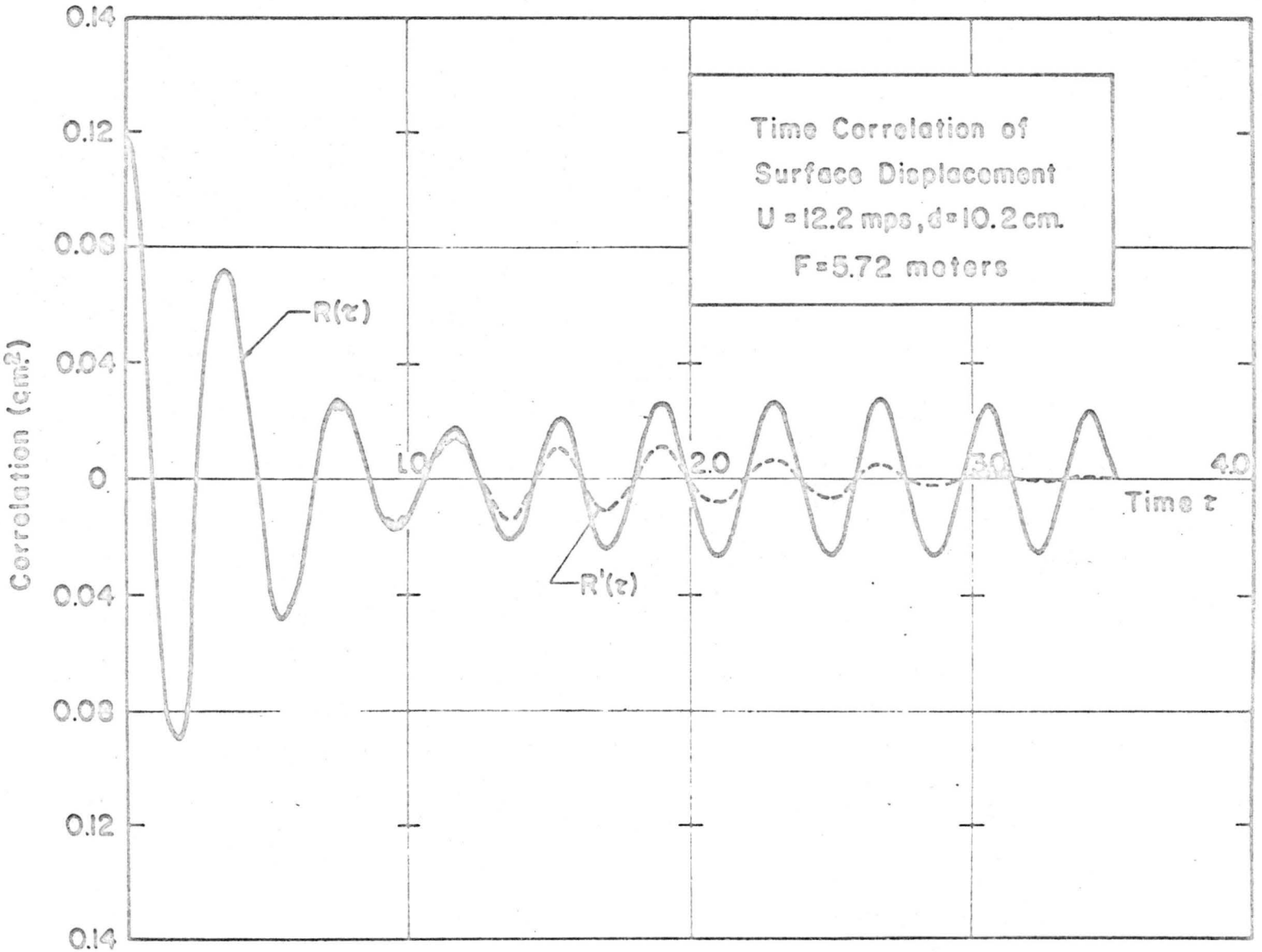

Figure 13. Typical unfaded and faded autocorrelation functions for the displacement of the water surface.

TABLE II

Case	$\bar{c}_e / \bar{\lambda}$	1/P	f_m
21	2.74	2.87	2.91
79	4.62	4.83	4.74
100	5.61	5.71	5.65
113	2.91	2.85	2.76
169	3.24	3.31	3.26

The energy spectra were calculated by means of the following relation:

$$\Phi(f) = \int_0^{\infty} R(\tau) \cos 2\pi f t \, dt \, . \qquad (11)$$

The scheme for evaluating the integral in Eq. (11) for a finite record is given by Blackman and Tukey, (1958). However, instead of the usual technique of "hanning," it was preferred to obtain a suitable lag window by multiplying the function $R(\tau)$ by:

$$g(\tau) = (1 + \cos \frac{\pi \tau}{T_m}) \, , \qquad (12)$$

where T_m for our data is 3.5. The fading function $g(\tau)$ has the advantage of suppressing the periodic component in the autocorrelation function at large lags without removing any information at short lags. An example of the faded autocorrelation $R'(\tau)$ $(=Rg)$ corresponding to the curve of $R(\tau)$ is shown in Figure 13.

The spectrum corresponding to the faded autocorrelation $R'(\tau)$ in Figure 13 is shown in Figure 14. Note that the tendency toward periodicity in the wave train also is indicated in this spectrum. Higher harmonics of the frequency f_m for which the energy is maximum appear as indicated in this Figure. If the waves were perfectly periodic, the idealized spectrum based on the $R(\tau)$ curve would develop as spikes of infinite height at n multiples of f_m. However, because the waves are not truly periodic, and because of the random components which exist in the signal, the spectrum actually takes the bumpy shape indicated in Figure 14.

Typical values of f_m are shown with corresponding values of 1/P and $\bar{c}_e/\bar{\lambda}$ in Table II. Because of the narrowness of the region containing most of the energy in the spectra for wind generated waves in the channel, these three frequencies are approximately equal. Thus, for practical

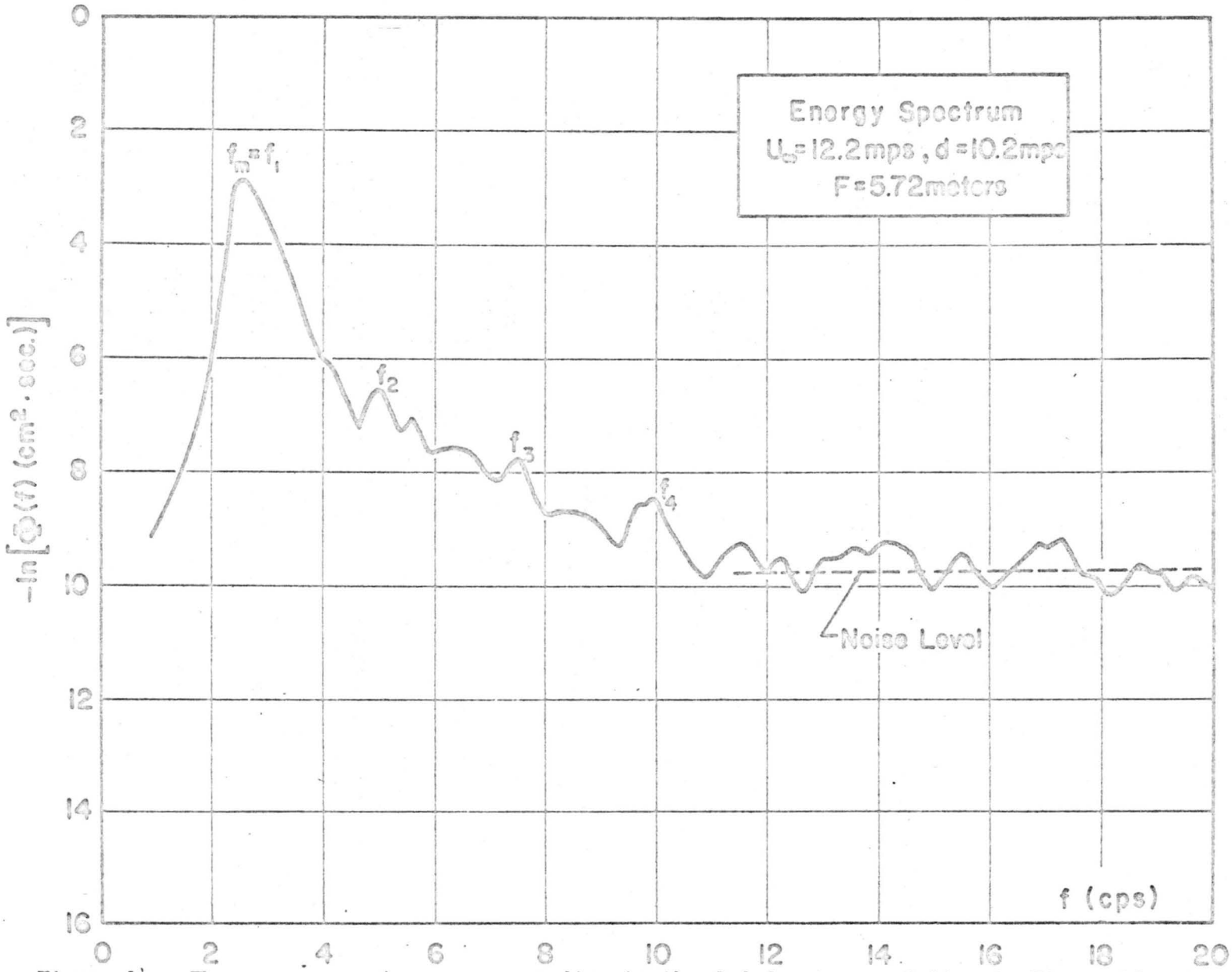

Figure 14. The energy spectrum corresponding to the faded autocorrelation in Figure 13.

purposes, the waves in the channel may be characterized essentially by the properties associated with the significant waves.

The Growth of Waves in the Channel

The frequency spectra calculated at different fetches for the same air velocity indicate how the waves grow as they move downstream along the channel. A typical set of spectra for increasing fetch is shown in Figure 15. These curves have been corrected by subtracting out the noise level, and have been smoothed by a method similar to that discussed by Hidy and Plate (1965). Near the leading edge of the water (small fetch), the observed spectrum contains little total energy and is rather sharp. As the waves travel downstream, the magnitude of the spectral density function increases, the primary peaks broaden at first, then tend to sharpen up while the values of f_m decrease.

The growth of waves in the range of higher frequencies tends to be limited as indicated in Figure 15. The complete mechanism for restraining the growth of the high frequency components is not known. However, it can be seen that the limitation in growth, in part, can be the result of attaining a balance between gains in energy input from the air and losses by dissipation. The dissipation of energy in small gravity-capillary waves is probably related to the action of viscosity and surface tension. The loss by viscous forces in waves is proportional to $(ak)^2$ (Lamb (1932)) where a is the amplitude of a wave. As proposed by Longuet-Higgins (1962a), the loss resulting from surface tension can be related to the drain of energy from larger waves when capillary ripples are formed near the crests of the larger components. This particular mechanism indicates that the energy loss is proportional to $(a^2_c k^3_c)$. The subscript c refers to the capillary ripple on the crest of a larger wave. If the interaction between components in the wave train is a second or higher order effect (e.g., Phillips (1963)), the action of dissipative processes should balance the input of energy from the air motion in such a way that the net energy at equilibrium is smaller the higher the frequency range. This seems to be suggested in the behavior of the spectra shown in Figure 15.

It is interesting to note that the growth of components in the lower frequency range, say $f \leq 3.5$ cps in Figure 15, is approximately exponential. Qualitatively, this type of growth has been predicted in the recent shearing flow theories of Miles (see, for example, Miles (1960)).

Similarity Shape of the Spectrum

An important feature which was also exhibited by many of the spectra for the channel waves was the tendency for growth in such a way that a similarity shape in the spectral density function is maintained. The frequency spectrum can be expressed, with Eq. (11) in normalized form, as:

(17)

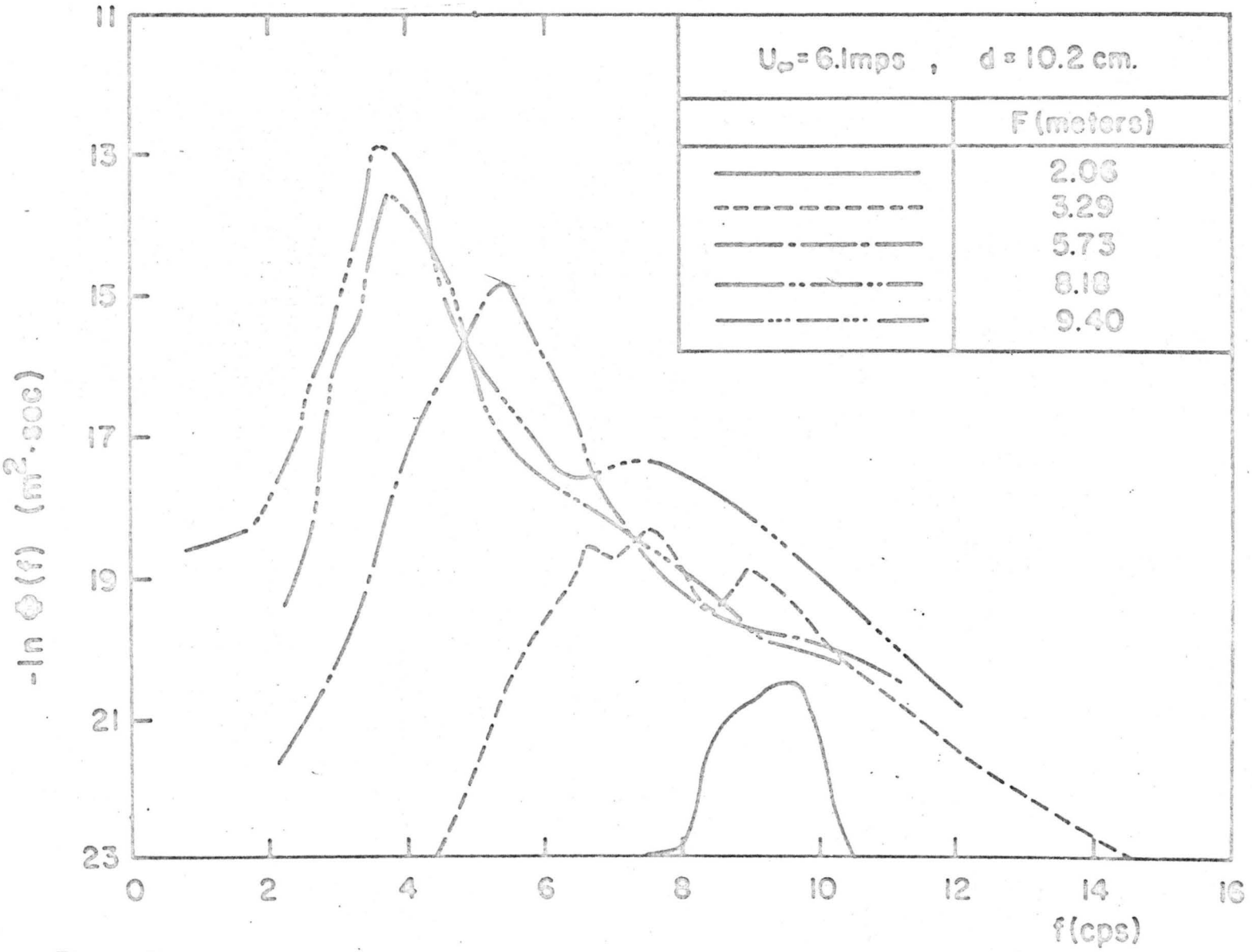

Figure 15. Growth of waves in the channel as indicated by the changes in frequency spectra with fetch.

$$\frac{\phi f_m}{\sigma^2} = \psi(f/f_m) \qquad (13)$$

where ψ denotes a dimensionless quantity representing a "universal" spectral density function.

Typical smoothed spectra which have been smoothed and corrected for noise level after Hidy and Plate (1965) are plotted in a form corresponding to Eq. (12) in Figure 16. The spectra in Figure 16 serve to define the similarity function ψ quite well. The conditions of U_{∞}, F and d for these spectra are shown in Table III along with the values of σ, f_m and ϕ_m. In general, it was found that the channel data followed ψ quite satisfactorily for the range 6 <U < 15 mps, and for 3 <F< 12 meters.

TABLE III

Case	d(meters)	U_{∞} (mps)	F(meters)	$\sigma \times 10^2$ (meters)	f_m(cps)	ϕ_m
163	0.0254	6.10	5.24	0.131	4.83	2.90×10^{-4}
175	0.102	10.7	10.7	0.767	2.36	7.99×10^{-3}
188	0.102	17.4	8.16	1.36	1.93	2.97×10^{-2}
192	0.0508	10.7	11.5	0.538	2.33	5.53×10^{-3}
208	0.0508	9.15	7.86	0.614	2.48	8.65×10^{-3}
212	0.102	10.7	5.74	0.457	3.17	4.15×10^{-3}

According to Phillips (1958a), on dimensional grounds, the equilibrium or saturation region in the high frequency region of the spectra for gravity waves should follow the f^{-5} rule. In contrast, it has been suggested by Hicks (see, for example, Phillips (1958b)) that the pure capillary spectrum should follow an $f^{-7/3}$ rule. As indicated in Figure 16, the dimensionless spectra for waves in the channel tend to follow the f^{-5} rule over approximately two decades in the high frequency range. In the highest frequency ratios, there is a tendency for some of the spectra to develop a slope less than -5. Capillary wave behavior should begin to appear above f = 13 cps in the frequency spectra. Only two cases, numbers 163 and 188 as shown in Figure 16, actually reach this range. For case 163, capillary waves should appear for f/f_m = 2.7 to 3.0, while, for case 188, f/f_m = 6.8 to 7.0. Thus, in Figure 16, these two examples may display the beginnings of a transition to the $f^{-7/3}$ range.

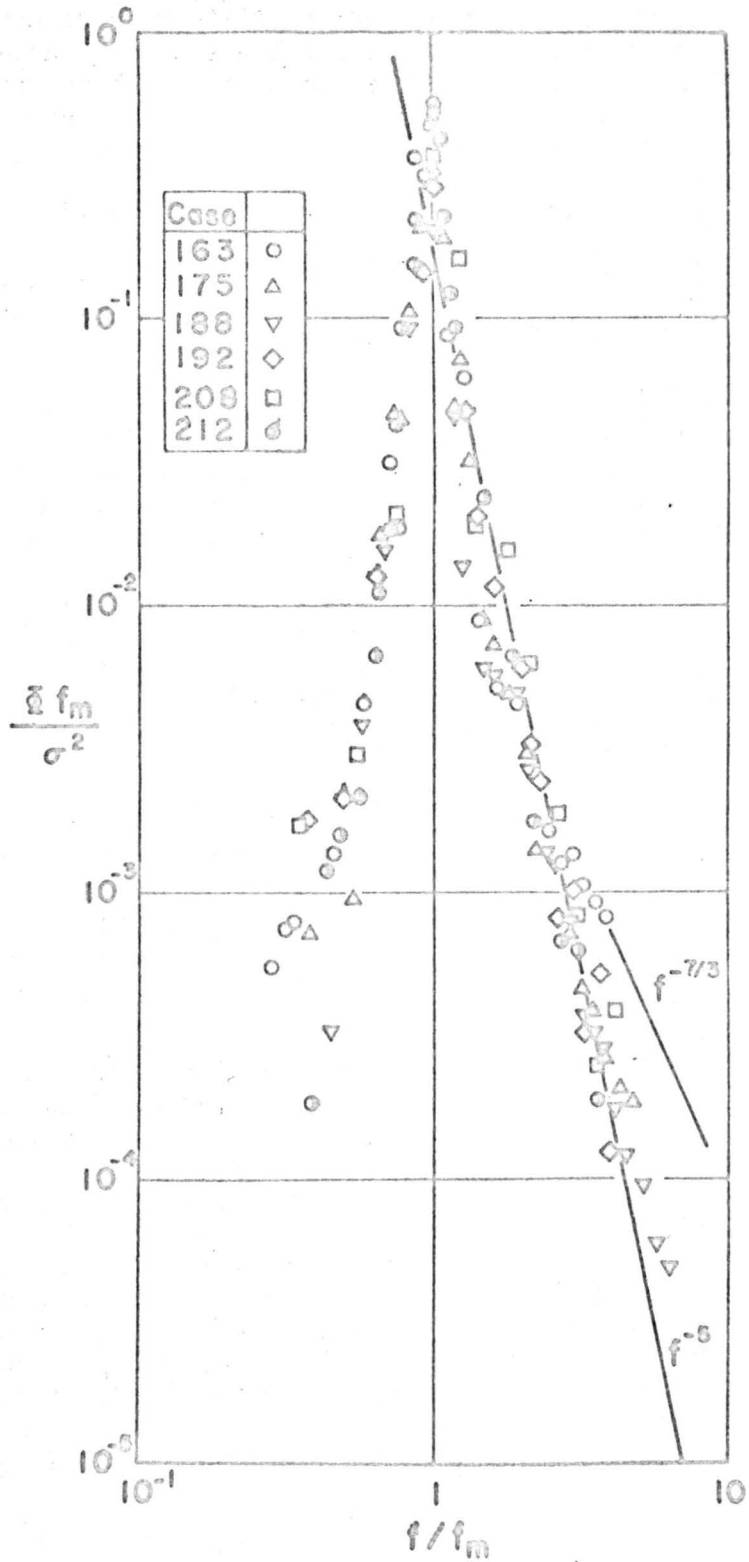

Figure 16. The similarity spectrum for wind generated waves in the channel. After Hidy and Plate (1965).

Unfortunately, the existence of the $f^{-7/3}$ rule cannot be verified generally in these results because the highest frequencies which can be resolved with some accuracy in the computation scheme used, lie around 15 cps. Therefore, these data cannot provide conclusive evidence for the existence of an equilibrium range in capillary waves.

VI. SOME COMPARISONS BETWEEN WAVES IN THE CHANNEL AND OCEAN WAVES

This study was not intended specifically to model waves at sea. Nevertheless, it is worthwhile to see where the data taken for the channel waves fit into the overall picture of wind generated waves.

The properties of the wind waves generated in the channel easily can be placed in perspective with much larger scale conditions by using well known pictures of wave behavior. As an illustration, the channel data have been plotted schematically in two "scaling" drawings of Hicks (1963), as shown in Figures 17A and B. In Figure 17A, the logarithm of the standard deviation is plotted against the logarithm of fetch. The numbers near curves or points refer to wind speeds taken in the field at somewhat different anemometer heights. The values of wind speed for our data correspond to U_{oo}. Our data for waves in the channel fit nicely into the extreme region of short fetch of this figure. Similarly, Figure 17B shows the variation in f_m with fetch. Again our results for small waves correspond to field data taken at very small fetch.

Another way of illustrating where the wave data for the channel fit into the geophysical picture comes from the correlation curves of Wiegel (1963). On dimensional grounds, the mean properties of wind generated waves (on deep water) should be related to a Froude parameter with the characteristic length being the fetch. This correlation shows essentially the variation in standard deviation, length of significant waves, and frequently with fetch.

Wiegel's results include data taken over an extremely wide range of conditions, which include results of some laboratory experiments and field studies on lakes and on the ocean.

A plot of a number of values of σ, $\bar{\lambda}$, and f_m for the waves in the CSU channel is shown in Figure 18 along with average curves estimated from Wiegel's Figure 6-5-7. The averaged curve for the correlation of standard deviation (or 0.33 times the significant wave height $H_{1/3}$) falls approximately along the mean of the data from this study. Furthermore, the lines of maxima and minima in σ, as estimated from Wiegel's correlation, encompass all of our values. It is interesting to note, however, that there is a systematic deviation with U_{oo} for the parameter $g\sigma/U_{oo}^2$ in Figure 18. This indicates that the Froude criterion gF/U_{oo}^2 cannot be the only parameter for modeling the mean displacement of the water surface. Furthermore, it is clear from the data in Figure 8 and the points for high wind velocity in Figure 18 that the water depth should be included in correlating heights for waves moving at finite depth in channels.

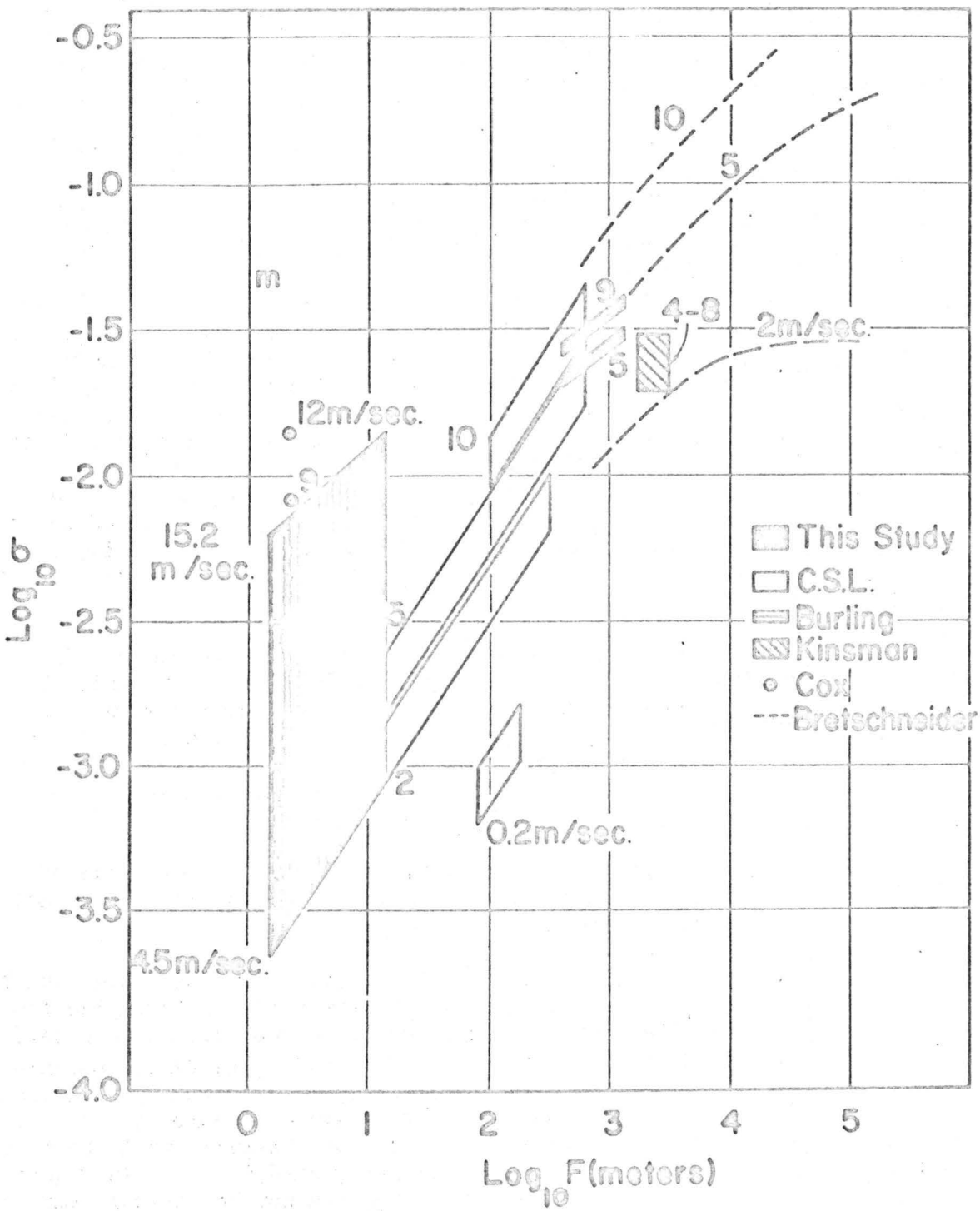

Figure 17A. Properties of small wind waves. Standard deviation. After Hicks (1963).

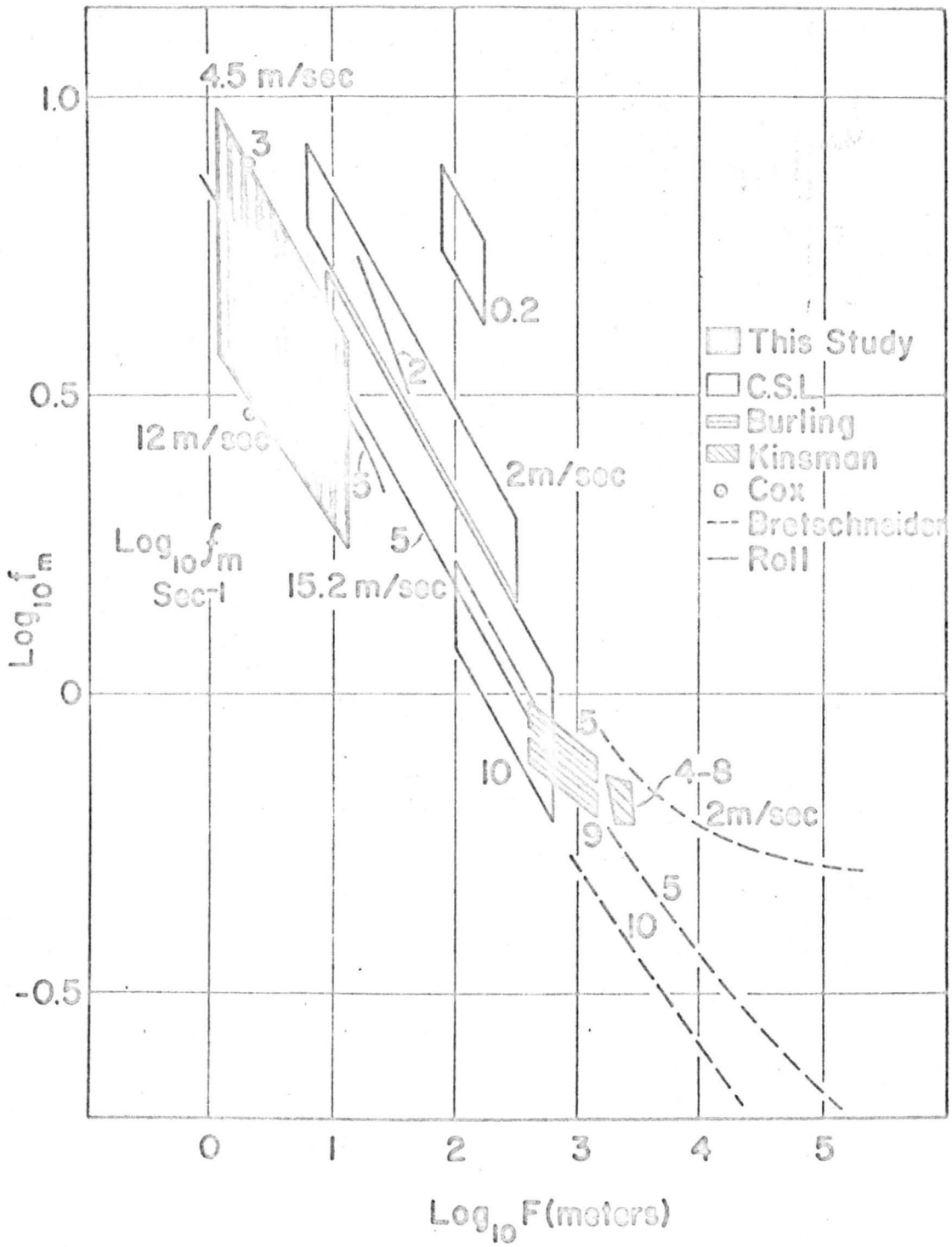

17B. Properties of small wind waves. Frequency of significant waves. After Hicks (1963).

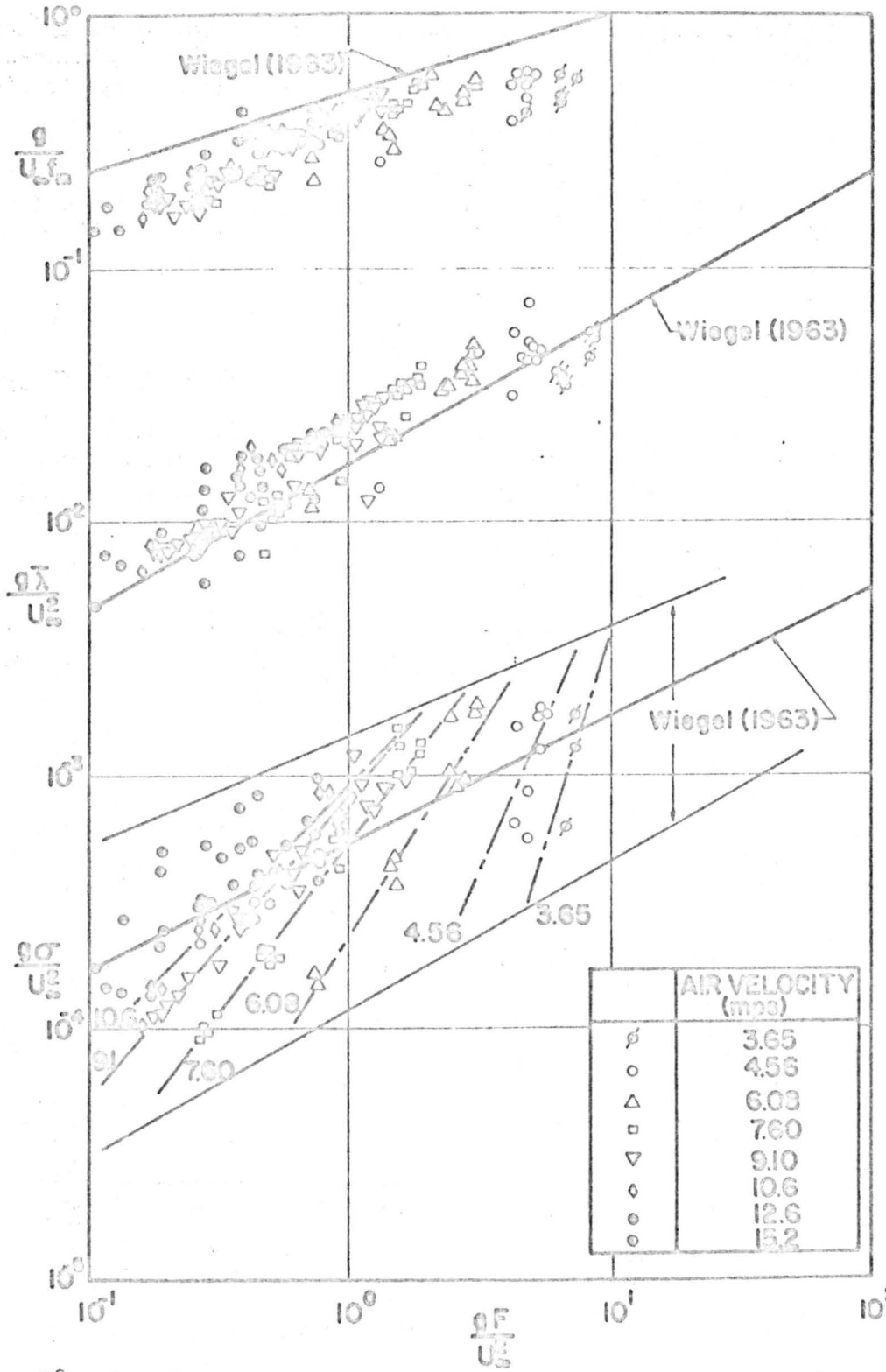

Figure 18. Froude number correlation of properties of wind waves. After Wiegel (1963).

The data for the dimensionless wave length of significant waves in the channel fit Wiegel's correlation curve satisfactorily. There is a tendency, however, for our points to lie somewhat above the estimate of Wiegel's line.

A plot of the wind tunnel data for f_m indicates that Wiegel's curve is again approached. However, in this case, our data lie somewhat below the estimated correlation curve. This is somewhat misleading, however, since comparatively little data is presented for this value (in terms of P) in Wiegel's paper.

The dimensionless energy spectrum derived by Eq. (12) can be compared to the dimensionless form discussed by Bretschneider (1963a and 1963b), provided that it is assumed that σ^2/f_m is approximately equal to $0.34\ \Phi_m$ where Φ_m is the maximum value of the spectral density function (see, for examples, the values in Table III). This has been done and the comparison is shown in Figure 19. Bretschneider's estimate for the Neumann spectrum corresponding to fully developed sea is shown along with our dimensionless spectrum. For further comparison, typical data of Burling as calculated by Bretschneider are shown in Figure 19. As might be expected, the dimensionless spectrum for waves at very short fetch in the channel is narrower than Burling's data taken at F $\simeq$ 1000 meters and the Neumann spectrum for nearly infinite fetch. The three dimensional character of waves developing on the surface of the oceans or lakes, of course, cannot be reproduced in the channel.

Acknowledgement

The wind-water tunnel at Colorado State University was constructed under a matching grant from the National Science Foundation. This work was supported by the National Science Foundation in connection with its grant to Colorado State University, and its contract with the National Center for Atmospheric Research. The authors are grateful to R. Biro, C. Goodwin, Hosein Shokouh, C. Yang and many others for their efforts in carrying out the experimental program and analyzing the extensive data of this study.

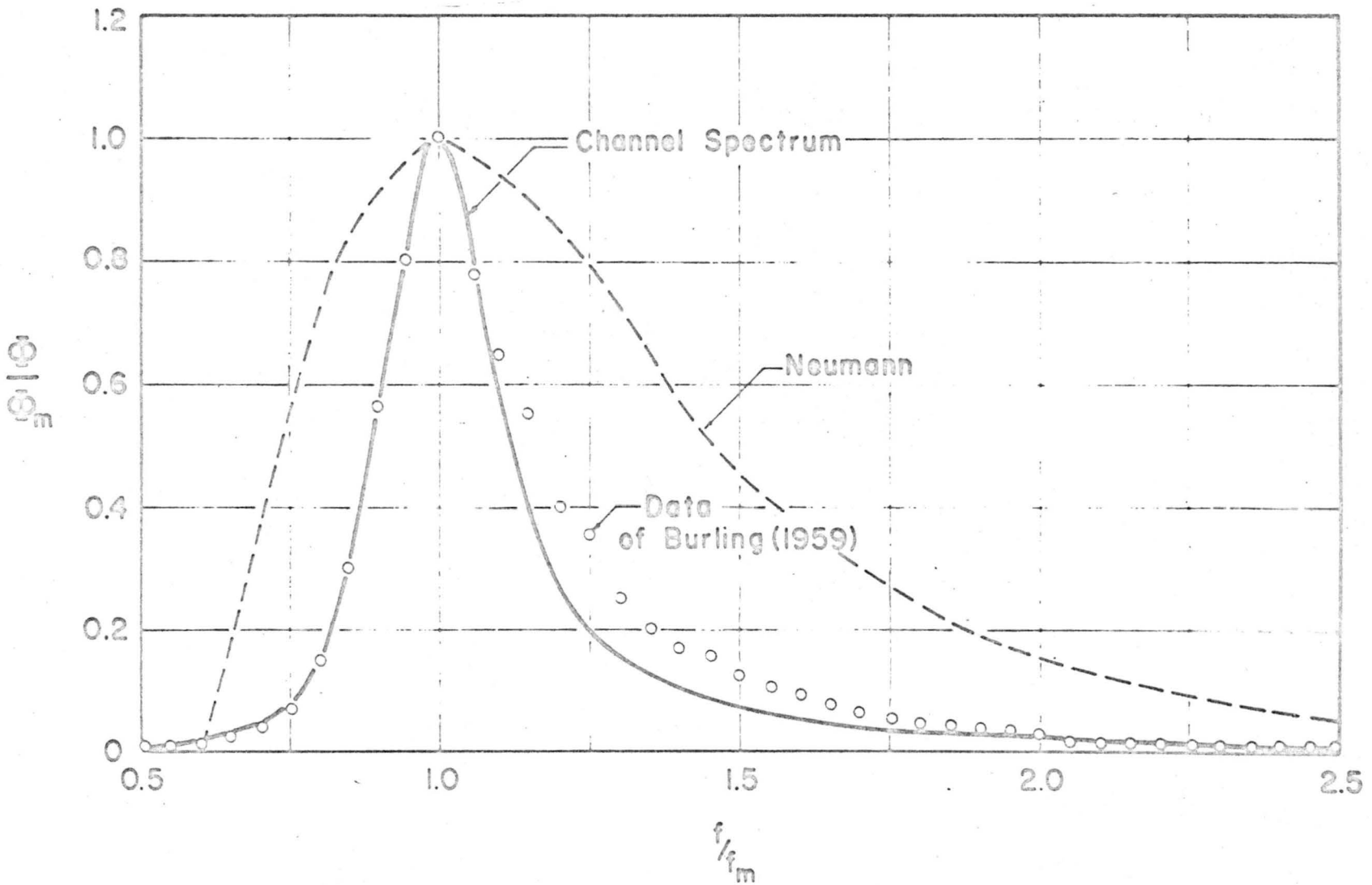

Figure 19. Comparison between dimensionless spectra for wind waves and the data of Burling for short fetch.

REFERENCES

Benjamin, T. B. 1959: Shearing flow over a wavy boundary. J. Fluid Mech. 6: 161-205.

Blackman, R.B. and J. W. Tukey 1958: The measurement of power spectra. Dover Publications, New York, 190 pp.

Bretschneider, C. L. 1963a: A one-dimensional gravity wave spectrum, in Ocean Wave Spectra. Prentice Hall, Inc., Englewood Cliffs, N. J., 357 pp.

1963b: Discussion of H. Walden's Comparison of one-dimensional wave spectra recorded in the German Bight with various "theoretical" spectra, in Ocean Wave Spectra. Prentice-Hall, Inc., Englewood Cliffs, N.J., 357 pp.

Cohen, L. S. and T. J. Hanratty 1965: Generation of waves in the co-current flow of air and a liquid. A.I.Ch.E. Journal, 11: 138-144.

Cox, Charles 1958: Measurements of slopes of high frequency wind waves. J. Mar. Res., 16: 199-225.

Fitzgerald, L. M. 1963: Wind-induced stresses on water surfaces; a wind tunnel study. Aust. J. Phys., 16: 475-489.

Francis, J. R. D. 1951: The aerodynamic drag of a free water surface. Proc. Roy. Soc. (London), A 206: 387-406.

Goodwin, C. R. 1965: The effect of wind drag on open-channel flow. Unpublished M. S. thesis, Colorado State University, Fort Collins, Colo., 93 pp.

Hicks, B. L. 1963: Estimation of the spectrum function for small wind waves, in Ocean Wave Spectra, Prentice-Hall, Inc. Englewood Cliffs, N. J. 357 pp.

Hidy, G. M. and E. J. Plate 1965: On the frequency spectrum of wind generated waves, to be published in Phys. of Fluids.

Keulegan, G. H. 1951: Wind tides in small closed channels. J. Res. Nat. Bur. Stand., 46: 358-381.

Lamb, H. 1932: Hydrodynamics. Dover Publications, New York. 738 pp.

Lilly, D. K. 1964: Personal communication.

Longuet-Higgins, M. S. 1962a: The generation of capillary waves by steep gravity waves. J. Fluid Mech., 16: 138-159.

1962b: The directional spectrum of ocean waves and processes of wave generation. Proc. Roy Soc. (London), 265A:286-317.

Miles, J. W. 1960: On the generation of surface waves by turbulent shear flows. J. Fluid Mech., 7: 469-478.

Phillips, O. M. 1958a: The equilibrium range in the spectrum of wind generated waves. J. Fluid Mech., 4: 426-433.

1958b: Comments on Dr. Cox's paper. J. Mar. Res., 16: 226-230.

1963: The dynamics of random finite amplitude gravity waves, in Ocean Wave Spectra, Prentice-Hall, Inc., Englewood Cliffs, N. J.,357 pp.

Schlichting, H. 1960: Boundary layer theory. 4th Ed., McGraw-Hill Book Co., Inc., New York, 647 pp.

Schooley, A. H. 1963: Simple tools for measuring wind fields above wind-generated water waves. J. Geophys. Res., 68:5497-5504.

Sekerzh-Zenkovich, Y. I. 1956: On the theory of stationary capillary waves of finite amplitude on the surface of a heavy fluid. Dokl. Akad. Nauk SSSR, 109:913-918.

Sheppard, P. A. 1952: Current research at Imperial College, London on the structure of turbulent flow, in Geophysical Research Directorate papers No. 19, USAF Cambridge Res. Center, Cambridge, Mass., 528 pp.

Sibul, O. 1955: Laboratory study of wind waves in shallow water. U.S. Army Corps of Engineers, Beach Erosion Board, Tech. Memo, No. 72, 35 pp.

Tucker, J. J., and H. Charnock 1955: A capacitance-wire recorder for small waves, in Proc. of the 5th Conference on Coastal Engineering, Council of Wave Research, University of California, Berkeley, California.

Wiegel, R. L. 1963: Some engineering aspects of wave spectra, in Ocean Wave Spectra. Prentice-Hall, Inc., Englewood Cliffs, N. J., 357 pp.

Ursell, F. 1956: Wave generation by wind, in Surveys in Mechanics. Cambridge University Press, 475 pp.